РОССИЙСКИЙ ГОСУДАРСТВЕННЫЙ ПЕДАГОГИЧЕСКИЙ УНИВЕРСИТЕТ им. А. И. ГЕРЦЕНА
HERZEN STATE PEDAGOGICAL UNIVERSITY of RUSSIA

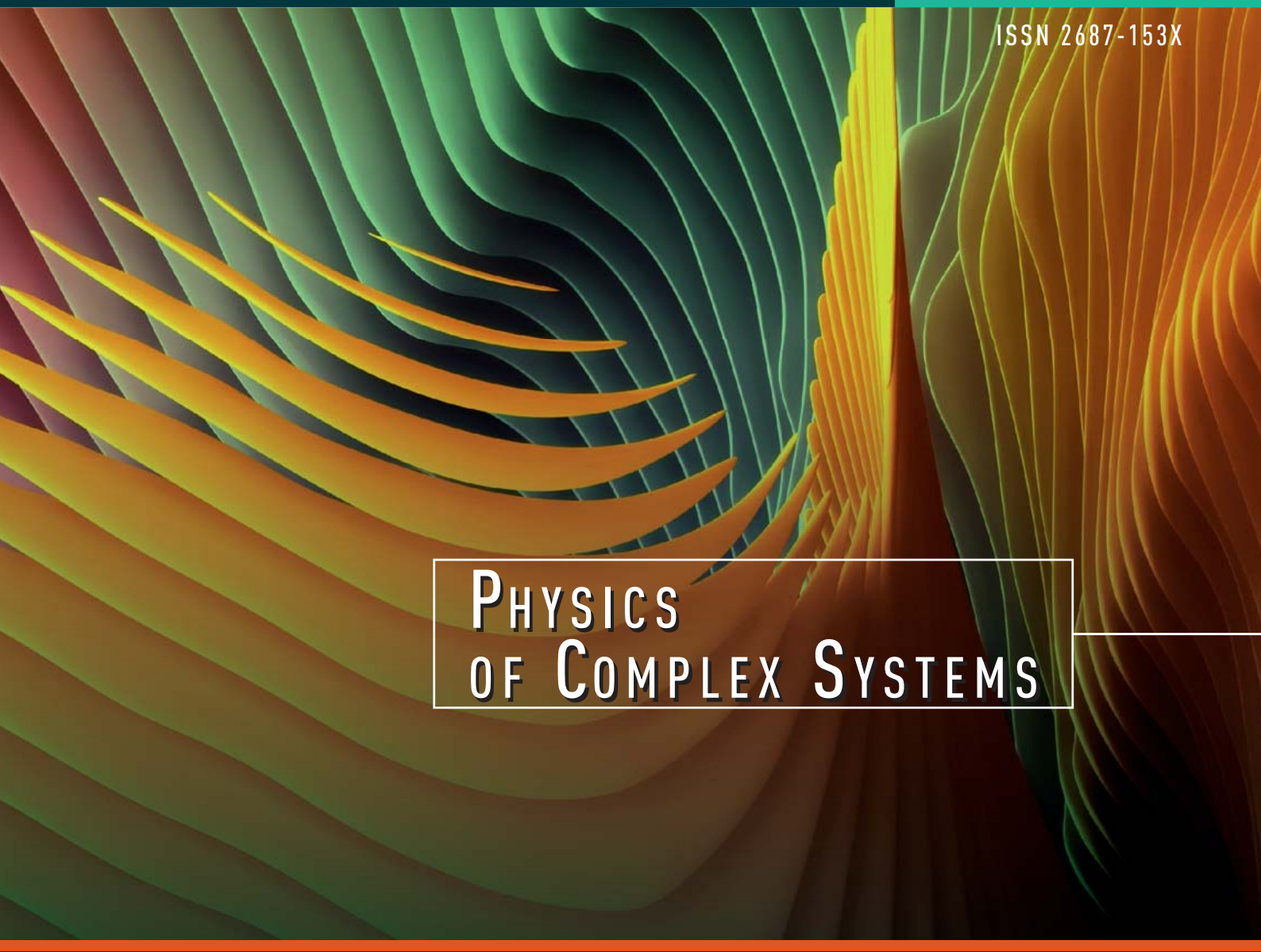

ISSN 2687-153X

Physics of Complex Systems

Т. 4 № 1 2023

Vol. 4 No. 1 2023

Herzen State Pedagogical University of Russia

ISSN 2687-153X (online)
physcomsys.ru
https://www.doi.org/10.33910/2687-153X-2023-4-1
2023. Vol. 4, no. 1

PHYSICS OF COMPLEX SYSTEMS

Mass Media Registration Certificate El No. FS77-77889, issued by Roskomnadzor on 10 February 2020
Peer-reviewed journal
Open Access
Published since 2020
4 issues per year

Publishing house of Herzen State Pedagogical University of Russia
48 Moika Emb., Saint Petersburg 191186, Russia
E-mail: izdat@herzen.spb.ru
Phone: +7 (812) 312-17-41

Data size 2,76 Mbyte
Published at 14.04.2023

Editors of the English text *M. V. Bumakova*
Corrector *D. A. Ivanov*
Cover design by *O. V. Rudneva*
Layout by *A. M. Khodan, L. N. Kliuchanskaya*

CONTENTS

Condensed Matter Physics. Dielectrics

UDC 538.9

EDN YRXKOW
https://www.doi.org/10.33910/2687-153X-2022-4-1-3-9

The role of polar relaxers in the formation of the piezoelectric state in the vinylidene fluoride-tetrafluoroethylene copolymer

Yu. A. Gorokhovatsky[1], D. E. Temnov[1], Yu. I. Sotova✉[1]

[1] Herzen State Pedagogical University of Russia, 48 Moika Emb., Saint Petersburg 191186, Russia

Authors

Yuriy A. Gorokhovatsky, ORCID: 0000-0001-5085-2525, e-mail: gorokh-yu@yandex.ru

Dmitry E. Temnov, ORCID: 0000-0002-9560-4346, e-mail: detem@yandex.ru

Yulia I. Sotova, ORCID: 0000-0001-6792-2390, e-mail: juliasotova1992@mail.ru

For citation: Gorokhovatsky, Yu. A., Temnov, D. E., Sotova, Yu. I. (2023) The role of polar relaxers in the formation of the piezoelectric state in the vinylidene fluoride-tetrafluoroethylene copolymer. *Physics of Complex Systems*, 4 (1), 3–9. https://www.doi.org/10.33910/2687-153X-2022-4-1-3-9 EDN YRXKOW

Received 15 January 2023; reviewed 10 February 2023; accepted 10 February 2023.

Funding: The research was supported by the Ministry of Education of the Russian Federation as part of state task (Project No. FSZN-2020-0026).

Abstract. In this work, the corona electret and piezoelectric states of vinylidene fluoride-tetrafluoroethylene (P(VDF-TFE)) copolymer films were studied to determine the correlation between these states. Previously, it was determined that in the objects under study there are two types of polar structures that differ in the values of activation energy and frequency factor. A detailed description of the application of a numerical method for processing experimental curves of thermally stimulated short-circuit currents, the Tikhonov method of weak regularization, which makes it possible to determine the parameters of polar structures of both types, is given. It is shown that the key role in the formation of the piezoelectric state in P(VDF-TFE) is played by polar structures with a lower activation energy.

Keywords: electret state, polyvinylidene fluoride, thermally activation spectroscopy, Tikhonov's weak regularization method, piezoelectric effect

Introduction

At present, the study of polymeric piezoelectric materials is of great interest. The most common representative of this class of materials is polyvinylidene fluoride (PVDF) and its copolymers with trifluoroethylene (P(VDF-TrFE)) and tetrafluoroethylene (P(VDF-TFE)) (Kalimuldina et al. 2020; Kunming et al. 2021; Lee et al. 2016). Interest in the study of these materials is due, on the one hand, to the wide possibilities of their application (in electroacoustics, medicine, biology, etc.) (Ma et al. 2005; Ribeiro et al. 2015) and, on the other hand, to the lack of a common opinion among researchers about the nature of the piezoelectric effect in these materials. Therefore, a variety of research in this area continues—both in order to find an explanation for the nature of the piezoelectric effect and in order to achieve the best piezoelectric characteristics of PVDF.

It is known that the crystalline phase of PVDF can exist in five different modifications, of which the polar β-phase is of the greatest interest because of its piezoelectric properties (Singh et al. 2018). Since in order to impart piezoelectric properties to polymeric materials based on PVDF their preliminary polarization is necessary (one of the most common methods is polarization in the field of a corona discharge), as a rule, an electret (corona electret) state is formed in these polymer films along with the piezoelectric state (Park 2021).

The purpose of this study was to investigate the correlation between the corona electret and piezoelectric states in the P(VDF-TFE) copolymer.

Samples and research methods

In this work, the P(VDF-TFE) copolymer films (F2ME trademark) with a thickness of 20 μm were studied. The polarized state was created in the samples using the corona discharge field in two ways. The first method is the traditional method of polarization in the field of a corona discharge: the sample is placed in the field of a corona discharge (with a negative polarity of the corona electrode, since it was experimentally found that the value of the surface potential turns out to be much higher during polarization in a negative corona), kept in it for 10 min (polarization temperature is 80 °C), and then cooled to room temperature in the same field. However, this method is associated with a high probability of electrical breakdowns at elevated temperatures, which, in turn, leads to mechanical damage to polymer films. The second polarization method, proposed earlier in (Sotova et al. 2022), consists in polarization in the field of a negative corona discharge at room temperature for 10 minutes, and then (without an applied field, in the open circuit mode) the sample is heated to 80 °C and cooled to room temperature.

The processes of relaxation of the corona electret state in P(VDF-TFE) were studied by the method of thermally stimulated short-circuit currents (TSC) using the experimental equipment TSC II from Setaram. The piezoelectric modulus d_{33} was measured by a quasi-static method using a D33meter instrument.

Experimental results and discussion

With the polarization of P(VDF-TFE) polymer films by the traditional method, it is possible to achieve values of the piezoelectric modulus d_{33} = 26 ± 1 pC/N. It is important to note that the obtained value of the piezoelectric modulus is not only sufficiently high (for polymeric piezoelectrics) but also has good stability (to verify this statement, the sample was held in a thermostat at the temperature of 70 °C for 2.5 hours).

Fig. 1 shows the TSC curves measured in P(VDF-TFE) polymer films traditionally polarized in a negative corona discharge field for various linear heating rates β (6 and 9 °C/min) during current measurement.

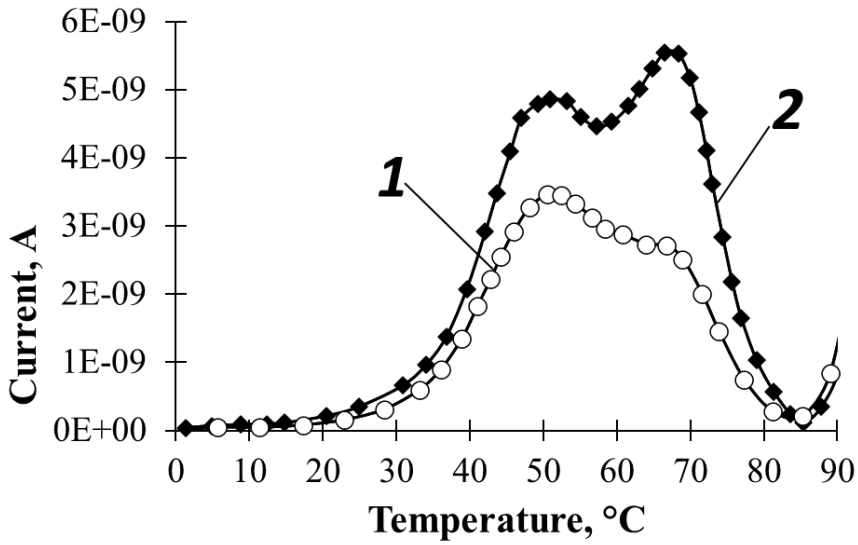

Fig. 1. TSC in P(VDF-TFE) films polarized in the field of a negative corona discharge at different linear heating rates (polarization temperature 80 °C): 1—linear heating rate β = 6 °C/min; 2—linear heating rate β = 9 °C/min

The TSC curves show two strongly overlapping peaks. Previously, a model of the P(VDF–TFE) polarization mechanism was proposed in (Gorokhovatsky et al. 2022): when the films are polarized in the field of a corona discharge, the negative homocharge is captured by deep near-surface traps. In the internal field of the homocharge, the orientation (and, importantly, the retention of the oriented state) of polar structures occurring in the composition of the ferroelectric phase of PVDF occurs (Kalimuldina et al. 2020). Two closely spaced peaks in Fig. 1 correspond to the processes of disorientation of polar structures (of two kinds), and the increase in the current above 85 °C is determined by the release of the homocharge from the traps.

 https://www.doi.org/10.33910/2687-153X-2022-4-1-3-9

There are several ways to process experimental TST curves to calculate the parameters of relaxers (activation energy W and frequency factor ω). One of the simplest and most common methods is the method of varying the heating rate, which is based on the dependence of the position of the TSC maximum on the heating rate: the higher the rate, the higher the temperature of the current peak maximum (Gorokhovatsky, Bordovskiy 1991). Knowing the temperature positions of the current maximum at various heating rates, it is possible to calculate the value of the activation energy and the frequency factor.

However, in this case, the method of varying the heating rate cannot be applied, since with an increase in the heating rate, the amplitude of the current maxima increases (both low-temperature and high-temperature peaks), but no shift to the region of high temperatures is observed. Apparently, this is due to the strong overlap of two closely spaced peaks.

To calculate the parameters of polar structures of both kinds, it makes sense to use Tikhonov's numerical method of weak regularization (Gorokhovatsky et al. 2018; 2022). For the experimental temperature dependence of the current, the activation energy distribution function *G(W)* is found, which is an inverse problem. The restoration of the distribution function for the activation energy *G(W)* is possible only in the case of a previously known value of the frequency factor. Since the frequency factor is not known in advance, a certain value of the frequency factor is chosen and the numerically reconstructed energy spectra are compared for two different heating rates of the same sample (ceteris paribus). In the case of a correctly chosen value of the frequency factor, the energy spectra (at least, the maxima of the distribution functions) should not differ for different heating rates. The difference in the reconstructed energy spectra indicates the need to select a different value of the frequency factor.

Figs. 2 and 3 show the reconstructed distribution functions for activation energy *G(W)*.

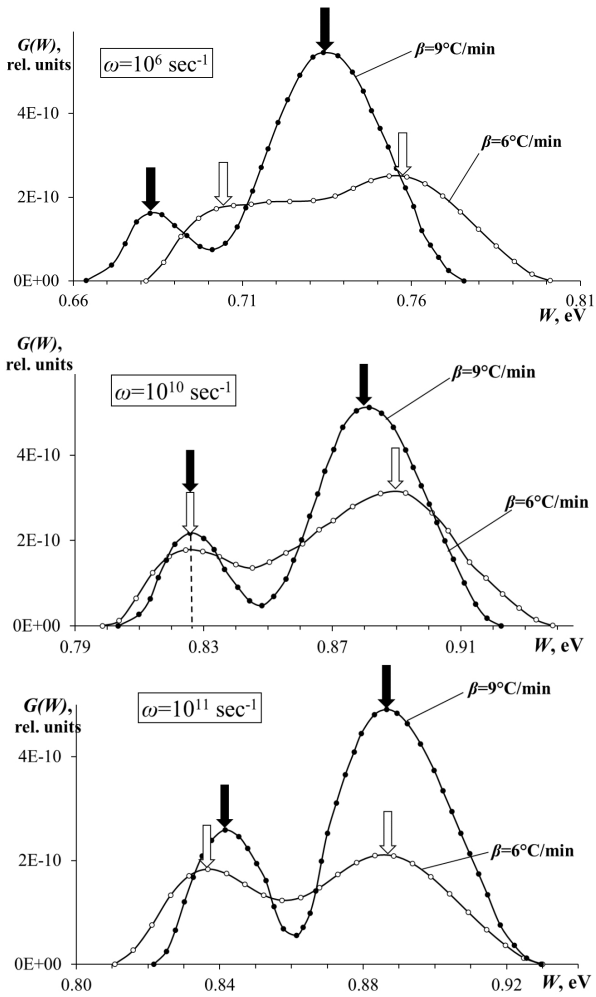

Fig. 2. Versions of the activation energy distribution functions G(W) for the P(VDF-TFE) copolymer polarized at a temperature of 80 °C in the field of a negative corona discharge for different linear heating rates. Calculation of activation energy and frequency factor for polar structures with lower activation energy

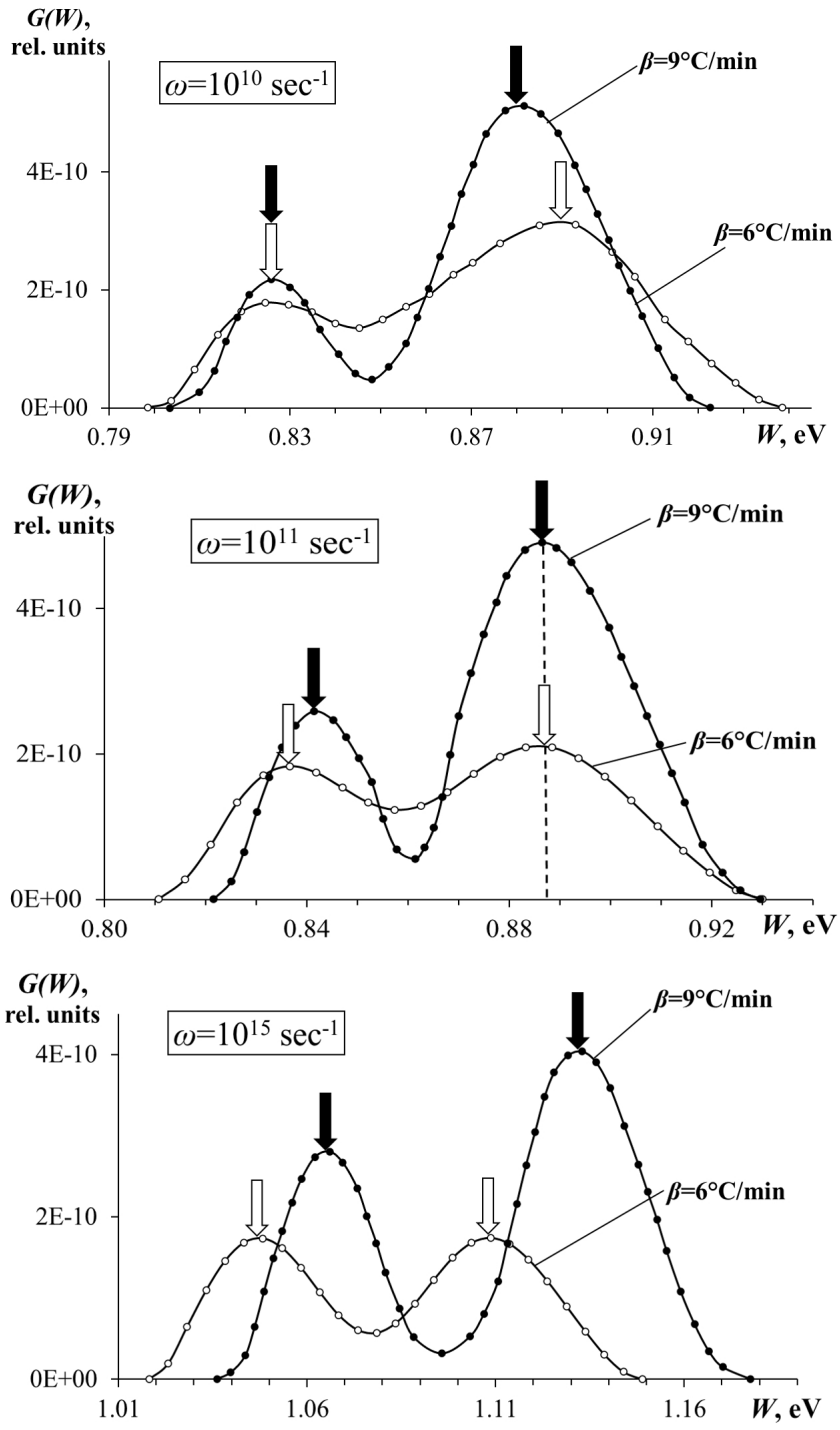

Fig. 3. Versions of the activation energy distribution functions G(W) for the P(VDF-TFE) copolymer polarized at a temperature of 80 °C in the field of a negative corona discharge for different linear heating rates. Calculation of activation energy and frequency factor for polar structures with higher activation energy

Fig. 2 shows that, according to Tikhonov's method of weak regularization, the parameters of polar structures with a lower activation energy are determined as W = 0.83 ± 0.04 eV, $\omega = 10^{10}$ sec^{-1} (with an accuracy of half a decade). According to Fig. 3, the parameters of polar structures with higher activation energy have the following values: W = 0.89 ± 0.04 eV, $\omega = 10^{11}$ sec^{-1} (accurate to half a decade). Thus, the polar structures in P(VDF-TFE) differ not only in the value of the activation energy but also in the value of the frequency factor (Gorokhovatsky et al. 2022).

 https://www.doi.org/10.33910/2687-153X-2022-4-1-3-9

Another method of polarization, proposed by us in (Sotova et al. 2022), consists in polarization in the field of a negative corona discharge at room temperature for 10 minutes with further heating (the sample is in the open circuit mode, without an applied external electric field) to a temperature of 80 °C and cooling up to room temperature. The values of the piezoelectric modulus d_{33} obtained with this method of polarization reach 22 ± 1 pC/N and are also characterized by good temperature stability.

Fig. 4 shows the TSC curves of P(VDF-TFE) polymer films polarized by the proposed method, measured at two different heating rates.

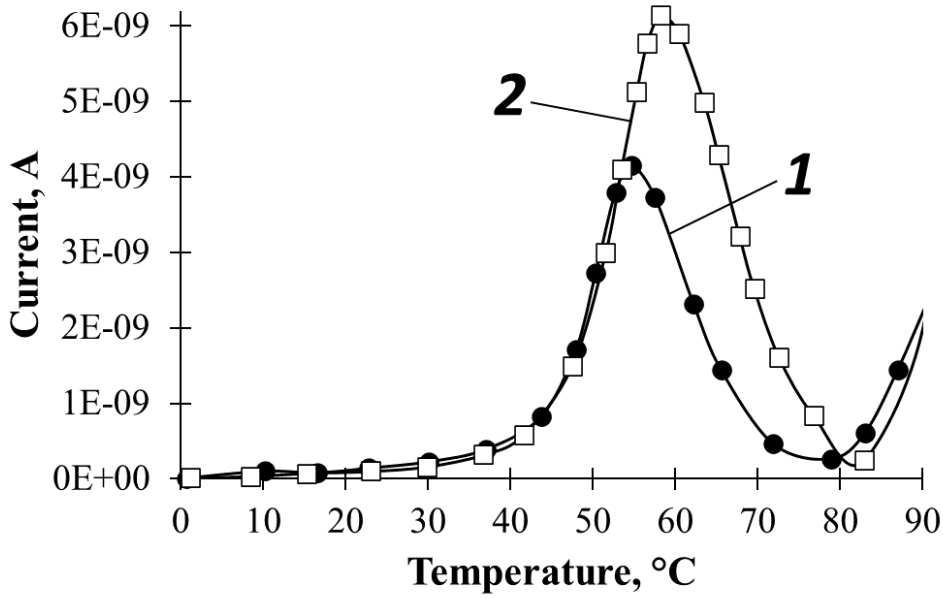

Fig. 4. TSC in P(VDF-TFE) copolymer films polarized at room temperature, depending on the linear heating rate (heating temperature after polarization is 80 °C): 1—linear heating rate β = 6 °C/min; 2—linear heating rate β = 9 °C/min

On the TSC curves in Fig. 4 there is one peak which is similar in its temperature position and magnitude to the low-temperature peak in Fig.1. Since it was previously concluded that the low-temperature peak in Fig. 1 is due to the misorientation of polar structures with lower activation energy, then we can assume that in this case the peak shown in Fig. 4 is due to the same process. The dependence of the TSC curves on the heating rate in this case has a traditional form: with an increase in the heating rate, the temperature position and the maximum of the current peak increase. The application in this case of the method of varying the heating rate gives the value of the activation energy W = 0.82 ± 0.03 eV, the frequency factor $\omega = 10^{10}$ sec^{-1} (with an accuracy of half a decade). The obtained values are in good agreement with the results calculated in the case of the traditional polarization method, which confirms that the peak in Fig. 4 is due to the misorientation of polar structures with lower activation energy.

Thus, during polarization in the field of a corona discharge at room temperature, the homocharge is captured by deep near-surface traps, and subsequent heating in the open circuit mode without an applied field leads to the orientation of polar structures (with lower activation energy) in the formed internal field of the homocharge. In this case, the resulting homocharge field turns out to be insufficient for the orientation of polar structures with higher activation energy. Apparently, the field of oriented polar structures with lower activation energy partially shields the homocharge field, thereby reducing it.

Comparison of the values of the piezoelectric modulus d_{33} (22 ± 1 pC/N) obtained using polarization in the field of a negative corona discharge at room temperature with the value of the piezoelectric modulus obtained by the traditional method of polarization in the field of a corona discharge at elevated temperature (26 ± 1 pC/N) allows us to conclude that the orientation of polar structures with lower activation energy is sufficient to create a stable piezoelectric state. The orientation of polar structures with higher activation energy only slightly increases the value of the piezoelectric modulus d_{33} and has little effect on its stability.

Conclusions

A high and stable value of the piezoelectric modulus d_{33} in P(VDF-TFE) polymer films can be achieved using a corona discharge field in various ways. It is possible to use the traditional technique and carry out polarization at an elevated temperature, as a result of which deep near-surface traps capture a homocharge, in the internal electric field of which the orientation and retention of the oriented state of polar structures occur. According to the TSC data, in this case, at least two kinds of polar structures are observed, which differ in their values of the activation energy W and the frequency factor ω. The numerical method of Tikhonov's weak regularization made it possible to determine the parameters of these relaxators: for polar structures with lower activation energy $W = 0.83 \pm 0.04$ eV, $\omega = 10^{10}$ sec^{-1} (with an accuracy of half a decade); for polar structures with higher activation energy $W = 0.89 \pm 0.04$ eV, $\omega = 10^{11}$ sec^{-1} (accurate to half a decade).

Another method of polarization in the field of a corona discharge is polarization at room temperature (which significantly reduces the probability of electrical breakdown) followed by heating and cooling (in open circuit mode, without an applied field). In this case, the homocharge is also captured by deep near-surface traps, but the resulting internal field of the homocharge is sufficient only for the orientation of polar structures with a lower activation energy, while the orientation of polar structures with a higher activation energy does not occur. Meanwhile, the piezoelectric modulus d_{33} obtained in this case, in terms of its value and temperature stability, is not inferior to the piezoelectric modulus obtained by the traditional polarization method. This allows us to conclude that the stability of the piezoelectric state in P(VDF-TFE) is associated with the orientation of polar structures with lower activation energy.

Conflict of Interest

The authors declare that there is no conflict of interest, either existing or potential.

Author Contributions

The authors have made an equal contribution to the paper.

References

Gorokhovatsky, Yu. A., Bordovsky, G. A. (1991) *Termoaktivatsionnaya tokovaya spektroskopiya vysokoomnykh poluprovodnikov i dielektrikov [Thermal activation spectroscopy of high-resistance semiconductors and dielectrics]*. Moscow: Nauka Publ., 248 p. (In Russian)

Gorokhovatsky, Yu. A., Sotova, Yu. I., Temnov, D. E. (2022) A study of charge relaxation in corona electrets based on P(VDF-TFE) copolymer. *Physics of Complex Systems*, 3 (3), 104–108. https://doi.org/10.33910/2687-153X-2022-3-3-104-108 (In English)

Gorokhovatsky, Yu. A., Temnov, D. E., Sotova, Yu. I. et al. (2018) Thermally stimulated depolarization data analysis: Simmons method and weak regularization method by Tikhonov. *Universitetskij Nauchnyj Zhurnal — Humanities and Sciences University Journal*, 37, 40–48. (In English)

Kalimuldina, G., Turdakyn, N., Abay, I. et al. (2020) A review of piezoelectric PVDF film by electrospinning and its applications. *Sensors*, 20 (18), article 5214. https://doi.org/10.3390/s20185214 (In English)

Kunming, S., Bin, C., Haiyang, Z. et al. (2021) Interface induced performance enhancement in flexible BaTiO3/PVDF-TrFE based piezoelectric nanogenerators. *Nano Energy*, 80, article 105515. https://doi.org/10.1016/j.nanoen.2020.105515 (In English)

Lee, C., Wood, D., Edmondson, D. et al. (2016) Electrospun uniaxially-aligned composite nanofibers as highly-efficient piezoelectric material. *Ceramics International*, 42 (2), 2734–2740. https://doi.org/10.1016/j.ceramint.2015.10.170 (In English)

Ma, Z., Kotaki, M., Inai, R., Ramakrishna, S. (2005) Potential of nanofiber matrix as tissue-engineering scaffolds. *Tissue Engineering*, 11 (1-2), 101–109. https://doi.org/10.1089/ten.2005.11.101 (In English)

Park, C. (2021) Electrets: A remedy for partial discharge caused by power electronics switching. *IEEE Transactions on Industrial Electronics*, 68 (12), 12947–12952. https://doi.org/10.1109/TIE.2020.3045707 (In English)

Ribeiro, C., Sencadas, V., Correia, D. M., Lanceros-Mendez, S. (2015) Piezoelectric polymers as biomaterials for tissue engineering applications. *Colloids and Surfaces B: Biointerfaces*, 136, 46–55. https://doi.org/10.1016/j.colsurfb.2015.08.043 (In English)

Singh, H. H., Singh, S., Khare, N. (2018) Enhanced β-phase in PVDF polymer nanocomposite and its application for nanogenerator. *Polymers for Advanced Technologies*, 29 (1), 143–150. https://doi.org/10.1002/pat.4096 (In English)

Sotova, Yu. I., Gorokhovatsky, Yu. A., Temnov, D. E. (2022) The role of the electret effect in the formation of the piezoelectric state in the polyvinylidene fluoride-tetrafluoroethylene copolymer films. *Nauchno-tekhnicheskie vedomosti SPbGPU. Fiziko-matematicheskie nauki — St. Petersburg Polytechnical State University Journal. Physics and Mathematics*, 15 (2), 8–16. https://doi.org/10.18721/JPM.15201 (In English)

Condensed Matter Physics. Dielectrics

UDC 53.08, 538.9+539.23

EDN QBUBEL
https://www.doi.org/10.33910/2687-153X-2022-4-1-10-16

Electrophysical properties of polymer membranes with the introduction of rare-earth metal compounds into membrane matrix

N. A. Lapatin✉[1], R. A. Castro Arata[1], E. A. Karulina[1], T. V. Reztsov[1]

[1] Herzen State Pedagogical University of Russia, 48 Moika Emb., Saint Petersburg 191186, Russia

Authors

Nikolay A. Lapatin, ORCID: 0000-0002-6306-2968, e-mail: nicoljapat@mail.ru

Rene Alejandro Castro Arata, ORCID: 0000-0002-1902-5801, e-mail: recastro@mail.ru

Elena A. Karulina, ORCID: 0000-0001-9604-4769, e-mail: karulina@mail.ru

Tikhon V. Reztsov, ORCID: 0000-0003-2025-0579, e-mail: sunnyundeadjuvati@icloud.com

For citation: Lapatin, N. A., Castro Arata, R. A., Karulina, E. A., Reztsov, T. V. (2023) Electrophysical properties of polymer membranes with the introduction of rare-earth metal compounds into membrane matrix. *Physics of Complex Systems*, 4 (1), 10–16. https://www.doi.org/10.33910/2687-153X-2022-4-1-10-16 EDN QBUBEL

Received 14 December 2022; reviewed 10 February 2023; accepted 10 February 2023.

Funding: The research was supported by the Ministry of Education of the Russian Federation as part of a state task (project No. FSZN-2020-0026).

Abstract. The original and modified with terbium(III) chloride perfluorosulfonic membranes were studied by dielectric spectroscopy in a wide range of frequencies (f = 10^0 Hz…10^5 Hz) and temperatures (T = 273 K…403 K). The membrane was modified by ion exchange sorption from an aqueous salt solution for several hours until an equilibrium value was reached. The sorption control was spectrophotometric. During the study, we obtained conductivity data of the samples and discovered their hopping conduction mechanism.

Measurement of the dielectric loss factor ε" in the layers of the sample made it possible to reveal the existence of a process leading to relaxation losses in the samples.

Keywords: perfluorosulfonic membrane, modification, rare earth elements, dielectric spectroscopy, conductivity

Introduction

Perfluorosulfonic membranes belong to a special type of polymer porous structures, the framework of which is formed by a fluorocarbon skeleton and ether chains. Cavities and channels are formed inside the membrane structure. The inner surface of these channels has polar functional groups: $–SO_3^-$–COO^-, etc. Membranes can be in protonated and ionic forms, such as K or Na. Currently, membrane of this type is used in fuel cells as a solid electrolyte. At the same time, perfluorosulfonic membranes have such useful properties as high proton conductivity, chemical and mechanical inertness to aggressive environments. The temperature range of membrane exploitation is relatively small. It is 290–363 K. A higher or lower temperature leads to a violation of the porous structure and of the integrity. The conductivity of the membrane also decreases. Modifications of such membranes with substances of organic and inorganic nature make it possible to increase the mechanical and thermal stability and to maintain or even increase proton conductivity at high temperatures and low relative humidity.

It is known that the introduction of mineral acids into membranes leads to an increase in the proton conductivity, but does not lead to an increase in the thermal stability. And it is an important factor in a membranes' exploitation (Napoli et al. 2013). In another study, substances of inorganic origin (SiO_2, TiO_2) were introduced into membranes. This allows to maintain the membrane conductivity at high temperatures (393 K) (Safronova, Yaroslavtsev 2015).

In the available body of literature, there is not much information devoted to studying the properties of membranes modified with composites of rare earth metals, which makes it possible to observe unique spectral and luminescent properties. It is also of interest to study the electrophysical properties of polymer systems based on conclusion of rare-earth metal composites in the membrane matrix. For example, the lanthanides have a polarizing effect on water inside membranes. This leads to changes in the conductivity of the resulting systems.

Samples and research methods

In our study, we investigated perfluorosulfonic membranes (MF-4SK type, PlastPolimer LLC, Saint Petersburg, Russia). Thicknesses of the samples were 170–200 micrometers.

Dielectric spectroscopy was chosen as a research method. The spectra were taken using the Concept-81 setup in the frequency range f = 100 Hz…105 Hz and in the temperature range T = 273 K…403 K. The experiment was carried out on the Concept 41 setup (Novocontrol Technologies GmbH & Co). The setup consists of a frequency impedance analyzer (frequency range: 3×10^{-6} Hz – 20×10^{6} Hz), a measuring cell, a temperature control system (temperature range: –100 °C – +250 °C), an automatic data acquisition system, and a Dewar vessel with an evaporation and nitrogen gas supply system. We also studied the temperature dependence of the conductivity for the original and modified samples. The temperature dependence of the logarithm of the current was obtained on a TSC-II setup (Setaram) in the mode in which the sample is placed in a constant field during linear heating.

Chemical modification of the membrane was carried out by keeping the sample in an aqueous solution of $TbCl_3$ for 90 minutes. The concentration of the solution is 10^{-3} mol/l. Sorption control was carried out by using the spectrophotometric method on a Shimadzu UV-2550 spectrophotometer. And it was determined by the intensity of the absorption peak of terbium (λ_{max} = 219 nm).

Experimental results and discussion

As a result of the experiment, the frequency dependences of the specific conductivity σ of the original and modified MF4-SK membranes were obtained at different temperatures (Figs. 1, 2).

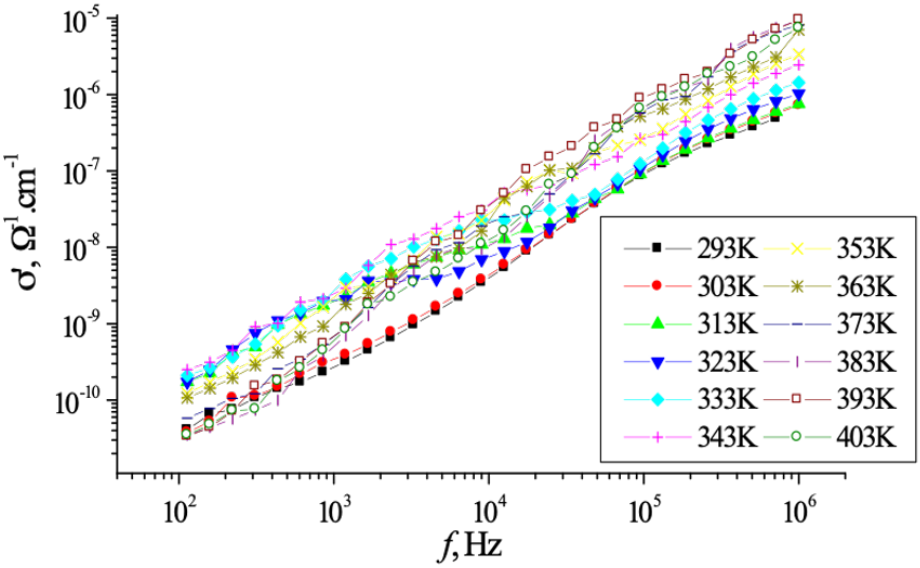

Fig. 1. Frequency dependencies of the specific conductivity σ' for samples of the MF-4SK system at different temperatures

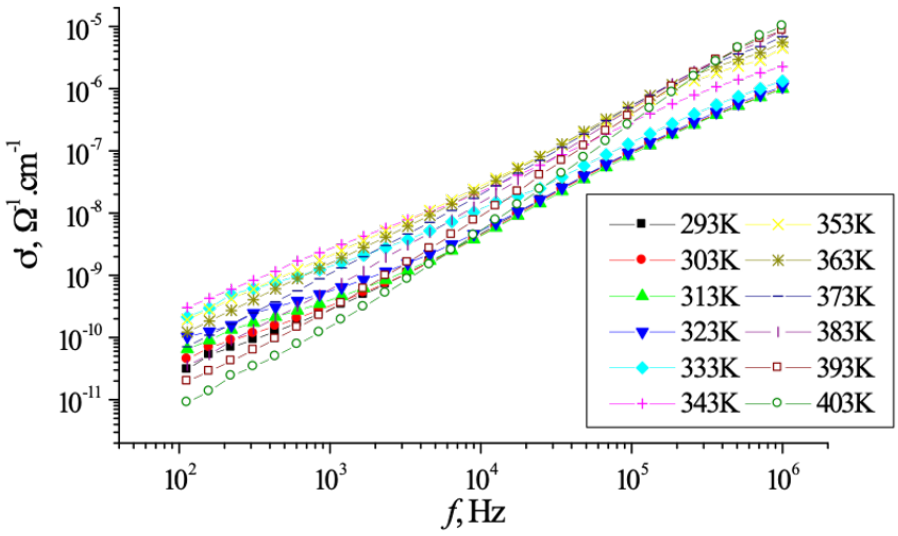

Fig. 2. Frequency dependencies of the specific conductivity σ' for samples of the MF-4SK+Tb system at different temperatures

The obtained frequency dependence of the conductivity obeys a power law. An analysis of the literature data has shown that this dependence is characteristic of most amorphous and crystalline semiconductors. And it is observed in many disordered systems characterized by hopping conductivity (Ivanchev et al. 2012). It can be assumed that when the membrane is modified with a terbium salt, the conductivity of the membrane increases at high temperatures because of an enhancement of water dissociation in the composition of aquated terbium ions $[Tb(H_2O)n]^{3+}$. As a consequence, the number of protons and their mobility in the system increase. The power-law characteristics of the frequency dependence σ and characteristics of the temperature dependence of the exponent s (Fig. 3) indicate the existence of a hopping mechanism of conduction in the frequency and temperature range under study.

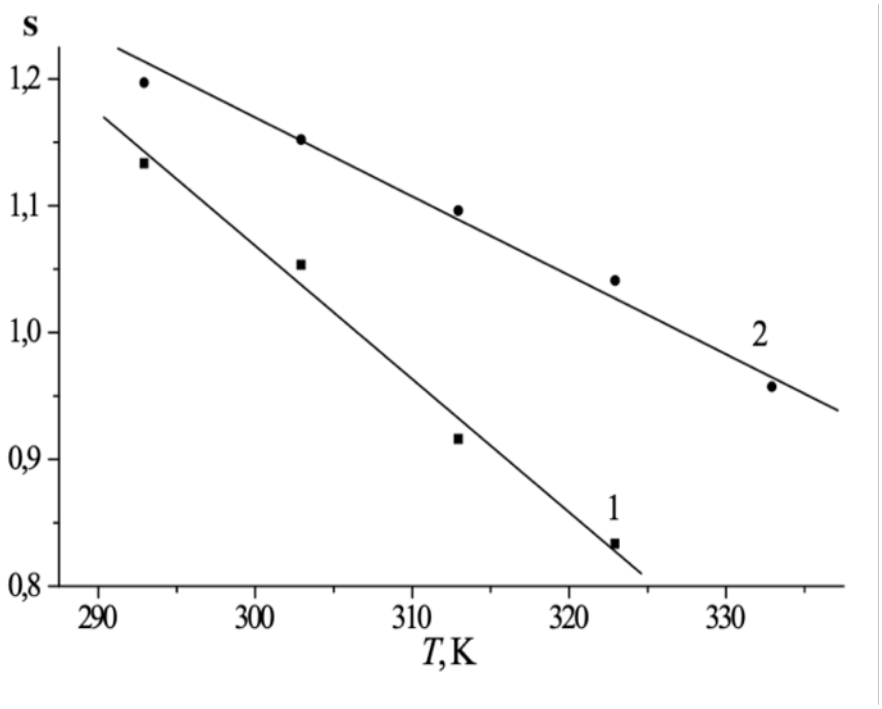

Fig. 3. Temperature dependencies of the exponent s. 1—original sample, 2—modified sample

 https://www.doi.org/10.33910/2687-153X-2022-4-1-10-16

The proton nature of the sample conductivity was confirmed by studying the temperature dependence of the transfer parameters using the experimental setup TSC-II (Setaram) (Fig. 4).

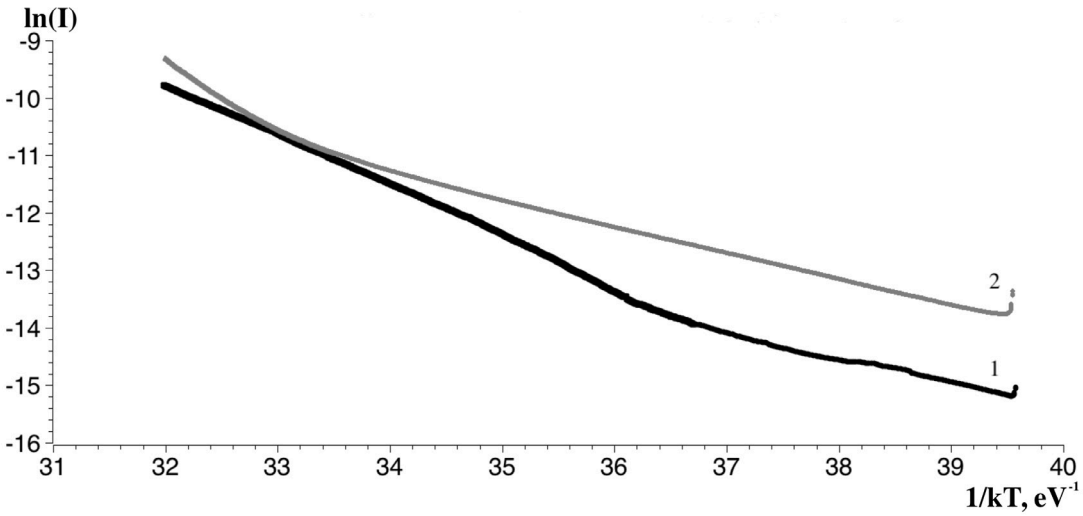

Fig. 4. Dependencies of the logarithm of the current on the reciprocal temperature. 1—original sample, 2—modified sample

For the original sample, a change in conductivity was observed in the region of 36.7 eV^{-1} (corresponding to a temperature of 316.2 K). For the modified sample, a shift in conductivity to higher temperatures is observed and corresponds to a value of 33.5 eV^{-1} (346.1 K). There is a shift in the region of critical temperatures during the modification of films, as in the case of the dispersion of the specific conductivity in an alternating field.

The data collected during the pilot study of the dielectric loss factor ε" in the original and modified samples revealed the existence of a maximum of this value in the medium frequency region. Data were obtained at various temperatures. Collected data indicate the existence of a process leading to relaxation losses in the samples (Figs. 5, 6). (Mustafaeva 2008).

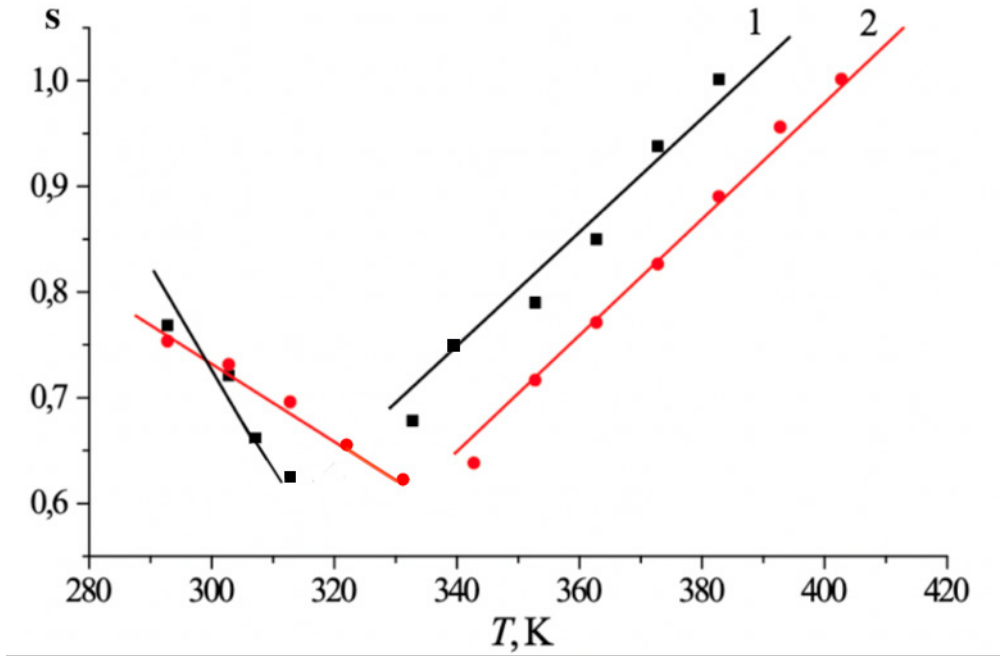

Fig. 5. Temperature dependencies of the exponent *s* for samples of two systems in normalized units of measurement. (1)—MF-4SK, (2)—MF-SK + Tb

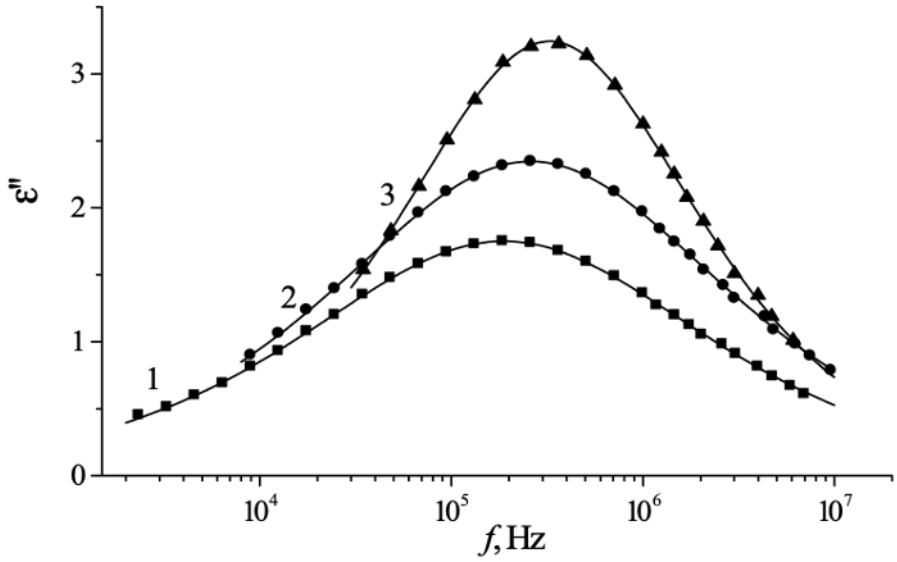

Fig. 6. Frequency dependencies of the complex permittivity's imaginary part (loss factor ε") for MF-4SK at different temperatures 1—303 K, 2—323 K, 3—333 K

The approximation of experimental curves (Figs. 6, 7) makes it possible to obtain values of the relaxation parameters within the Havriliak—Negami model: Δε, τmax, α, β.

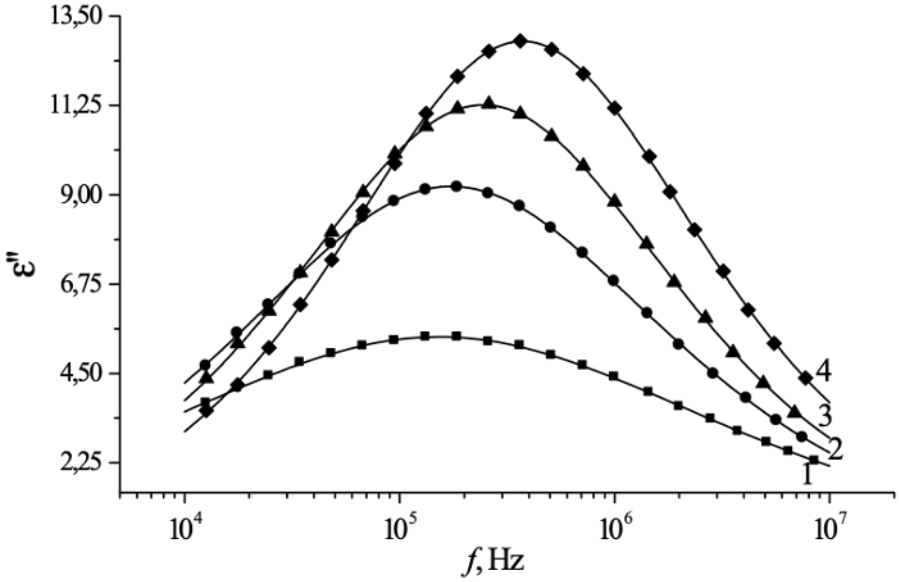

Fig. 7. Frequency dependencies of the imaginary part of complex permittivity (loss factor ε") for MF-4SK+Tb (process II) at different temperatures: 1—343 K, 2—353 K, 3—363 K, 4—373 K

https://www.doi.org/10.33910/2687-153X-2022-4-1-10-16

The obtained values indicate the existence of a distribution of relaxers over relaxation times in accordance with the Cole-Davidson and Cole-Cole models (Table 1).

Table 1. The values of the relaxation parameters of both systems, obtained by approximating the experimental dependences of the loss factor ε" on frequency at different temperatures

System	Temp.[K]	D_Eps	Tau-Max [s]	Alpha	Beta
MF-4SK	293	6.6150e + 00	1.047e – 06	5.7810e – 01	1.0000e + 00
	303	7.3550e + 00	8.464e – 07	5.6600e – 01	1.0000e + 00
	313	8.0440e + 00	9.291e – 07	5.4930e – 01	9.8960e – 01
	323	9.5670e + 00	6.134e – 07	5.8080e – 01	1.0000e + 00
	333	1.0250e + 01	4.872e – 07	7.1850e – 01	1.0000e + 00
	343	1.6570e + 01	3.731e – 07	6.8990e – 01	1.0000e + 00
	353	2.1960e + 01	2.901e – 07	6.8210e – 01	1.0000e + 00
MF-SK + Tb	343	2.8150e + 01	1.045e – 06	4.6800e – 01	1.0000e + 00
	353	3.6900e + 01	9.136e – 07	6.0250e – 01	9.3130e – 01
	363	4.0700e + 01	6.481e – 07	6.4380e – 01	1.0000e + 00
	373	4.4010e + 01	4.256e – 07	6.7600e – 01	9.8940e – 01
	383	4.4830e + 01	3.268e – 07	7.2910e – 01	1.0000e + 00

In the systems under study, fluorine-carbon, carbon-hydrogen fragments of the membrane core and polar sulfo groups found in the IR spectrum of the membranes can act as relaxers (Jonscher 1977). The activation energy of the relaxation process was determined from the temperature dependence of the most probable relaxation time. The results for the membranes of the two systems are presented in Table 2.

Table 2. The values of the activation energy of the relaxation process for films of two systems, obtained using the exponential Arrhenius law

System	Temperature range, K	E_a, eV	E_a, kcal/mol
MF–4SK	293…353	0.27 ± 0.02	6,21 ± 0,45
MF–4SK+Tb	343…383	0.42 ± 0.01	9,63 ± 0,20

Conclusions

All in all, the study of the electrophysical properties of polymer membranes with the addition of compounds of the rare earth metal (terbium) to their matrix made it possible to fix the hopping mechanism of charge transfer for both pure and modified membranes. The dispersion of the dielectric loss factor is characterized by the presence of the maximum of this parameter in the medium frequency range. The observed differences in the values of the polarization parameters for the films of the two systems are explained by the structural changes. The original polymer is going through these changes when it is modified with a terbium.

Conflict of Interest

The authors declare that there is no conflict of interest, either existing or potential.

Author Contributions

N. A. Lapatin modified the membrane and analyzed the dielectric spectra; R. Castro investigated the membrane using the method of dielectric spectroscopy and analyzed the spectra; E. A. Karulina analyzed the dielectric spectra; T. V. Reztsov conducted the experiment on the TSC-II facility.

All the authors discussed the final work and took part in writing the article.

References

Ivanchev, S. S., Likhomanov, V. S., Primachenko, O. N. et al. (2012) Nauchnye osnovy novoj tekhnologii polucheniya perftorirovannogo polimernogo elektrolita dlya toplivnykh elementov [Scientific principles of a new process for manufacturing perfluorinated polymer electrolytes for fuel cells]. *Membrany i membrannye tekhnologii — Membranes and membrane technologies*, 2 (1), 3–12. (In Russian)

Jonscher, A. K. (1977) The 'universal' dielectric response. *Nature*, 267, 673–679. https://doi.org/10.1038/267673a0 (In English)

Mustafaeva, S. N. (2008) Dielektricheskie svojstva monokristallov TlGa1–xFexSe2 v peremennykh elektricheskikh polyakh [Dielectric properties of TlGa1-xFexSe2 single crystals in alternating electric fields]. *Zhurnal radioelektroniki — Journal of Radio Electronics*, 5, 1–11. (In Russian)

Napoli, L., Lavorante, M. J., Franco, J. et al. (2013) Effects on nafion® 117 membrane using different strong acids in various concentrations. *Journal of New Materials for Electrochemical Systems*, 16 (3), 151–156. (In English)

Safronova, E. Yu., Yaroslavtsev, A. B. (2015) Synthesis of MF-4SC composite membranes exhibiting an anisotropic distribution of zirconia and ion transport asymmetry. *Petroleum Chemistry*, 55 (10), 862–865. https://doi.org/10.1134/S0965544115100229 (In English)

Theoretical physics. Cosmology

UDC 524.8

EDN JTHSXS
https://www.doi.org/10.33910/2687-153X-2022-4-1-17-23

On particle collisions during gravitational collapse of Vaidya spacetimes

V. D. Vertogradov[✉1,2]

[1] Herzen State Pedagogical University of Russia, 48 Moika Emb., Saint Petersburg 191186, Russia
[2] The Special Astrophysical Observatory of the Russian Academy of Sciences, 65 Pulkovskoe Highway, Saint Petersburg 196140, Russia

Author
Vitalii D. Vertogradov, ORCID: 0000-0002-5096-7696, e-mail: vdvertogradov@gmail.com

For citation: Vertogradov, V. D. (2023) On particle collisions during gravitational collapse of Vaidya spacetimes. *Physics of Complex Systems*, 4 (1), 17–23. https://www.doi.org/10.33910/2687-153X-2022-4-1-17-23 EDN JTHSXS

Received 14 December 2022; reviewed 18 January 2023; accepted 18 January 2023.

Funding: The research presented in this paper was supported by the Russian Science Foundation, grant No. 22-22-00112. The research is part of the SAO RAS state-commissioned assignment Conducting Fundamental Science Research.

Abstract. The center-of-mass energy can be arbitrarily high in Schwarzschild spacetime if one considers the front collision of two particles, one of which moves along the so-called white hole geodesics and the other one along the black hole geodesic. This process can take place if one considers the gravitational collapse model. In this paper, we consider the well-known naked singularity formation in the Vaidya spacetime and investigate the question about two particle collision near the boundary of the collapsing cloud. The center-of-mass energy of the front collision is considered. One particle moves away from the naked singularity and the other one falls onto a collapsing cloud. We show that the center-of-mass energy grows unboundly if the collision takes place in the vicinity of the conformal Killing horizon.

Keywords: gravitational collapse, particles collision, Vaidya spacetime, naked singularity, conformal symmetry

Introduction

The center-of-mass energy of two particles collision can grow unboundly in the Kerr spacetime (Banados et al. 2009) if one of the particles is fine-tunned (the so-called critical particle (Tanatarov, Zaslavskii 2013). This effect was first proposed by Bañados, Silk and West and is called the BSW effect. The original version of this effect declares absence of the unbound energies in Schwarzschild and Reissner-Nordström spacetimes. However, it was shown that this effect is possible in Reissner-Nordström-anti-de Sitter spacetime (Zaslavskii 2012a). Despite the unbound center-of-mass energy, a distant observer will measure small amount of the energy due to this process in the Kerr spacetime (Harada et al. 2012) and an escaping particle will be able to carry away arbitrarely large amount of energy in Reissner-Nordström case (Zaslavskii 2012b).

In spite of the fact that the BSW effect is absent in the Schwarzschild spacetime, one can still obtain the unbound center-of-mass energy of two colliding particles (Grib, Pavlov 2015). Due to geodesic completeness, there must be geodesics which appear in our Universe from the region inside the gravitational radius, i.e., the so-called white hole geodesics. For example, geodesics for particles with negative energy in the Kerr metric are such geodesics (Grib et al. 2014; Vertogradov 2015). One can imagine the following situation: the first particle moves along the white hole geodesic away from the gravitational radius and the second particle moves along the black hole geodesics falling onto the black hole. As a result, one can observe the front collision in the vicinity of the event horizon and due to this process

the center-of-mass energy can grow unboundly. The problem is that the Schwarzschild black hole is an eternal one and if one follows the geodesic back, then it must appear from the collapsing cloud. So, to understand the front collision in the vicinity of the event horizon in the Schwarzschild spacetime, one must consider the gravitational collapse problem. The nature of the white hole geodesics can be explained by the naked singularity formation due to the gravitational collapse problem (Vertogradov 2021). The outcome of the gravitational collapse is not limited to a black hole but also a naked singularity (Dey et al. 2022; Joshi 2007; Joshi, Malafarina 2011). The naked singularity formation in the Vaidya spacetime has been considered in (Dwivedi, Joshi 1989). The gravitational collapse of the generalized Vaidya spacetime and the naked singularity formation has been investigated in (Mkenyeleye et al. 2014; Vertogradov 2016a; 2016b; 2018). In the case of the eternal naked singularity formation in the Vaidya spacetime (Vertogradov 2018; 2022a) the unbound center-of-mass energy is possible only in the vicinity of the singularity.

In this paper, we consider the following model: a particle moves along the non-spacelike, future-directed geodesic which terminates at the naked singularity in the past. When the apparent horizon forms, the particle is in the vicinity of the apparent horizon and outside it. At this time, the second particle, moving along the black hole geodesic, falls onto the black hole. As a result, we have a front collision of two particles. We estimate the center-of-mass energy of this process and find out where this process should take place to results in unbound energy collision.

This paper is organized as follows: in Sec. 2 we consider the well-known gravitational collapse model of the Vaidya spacetime and show the naked singularity formation. We also show that the geodesics can originate at this singularity. In Sec. 3 we introduce the coordinate transformation and consider the Vaidya spacetime in conformally static coordinates. In this case we investigate the center-of-mass energy of the two particle front collision. Sec. 4 is the conclusion.

The system of units $G = c = 1$ will be used throughout the paper. We use the signature $-, +, +, +$.

Naked singularity formation in the Vaidya spacetime

The Vaidya metric (Vaidya 1951) describes a dynamical spacetime instead of a static spacetime as the Schwarzschild or Reissner-Nordström metrics do. In the real world, astronomical bodies gain mass when they absorb radiation and they lose mass when they emit radiation. This means that the space-time around them is time-dependent. Papapetroo (Papapetrou 1985) showed that the Vaidya spacetime violates the cosmic censorship conjecture and contains a naked singularity. The line element in Eddington-Finkelstein coordinates has the following form:

$$ds^2 = -\left(1-\frac{2M(v)}{r}\right)dv^2 + 2dvdr + r^2 d\omega^2. \tag{1}$$

Here $M(v)$ is the time-depended mass of the black hole, $d\Omega^2 = d\theta^2 + sin^2\,\theta d\phi^2$ is the metric on unit sphere.

The apparent horizon equation is given by (Poisson 2004):

$$r_{ah} = 2M(v)\,. \tag{2}$$

The first shell collapses at $r = 0$ at the time $v = 0$ and the singularity forms at this time. The singularity is naked if at the time of the singularity formation $v = 0$ the apparent horizon doesn't form and there is a family of non-spacelike, future-directed geodesics which terminate at the central singularity in the past. Let's prove the last statement. For this purpose, we define the mass function as:

$$M(v) = \mu v,\ \ \mu > 0\,. \tag{3}$$

Here μ is a positive constant. Here, we just show that a naked singularity is possible. See (Dwivedi, Joshi 1989) for a substantive investigation of this model.

To prove the existence of a family of non-spacelike, future-directed geodesics which terminate at the central singularity in the past, one should consider the null radial geodesic, which, for the metric (1) with the mass condition (3) has the following form:

$$\frac{dv}{dr} = \frac{2r}{r-2\mu v}\,. \tag{4}$$

 https://www.doi.org/10.33910/2687-153X-2022-4-1-17-23

The solution $v = const$ doesn't suit us because for infalling matter $v = const$ corresponds to ingoing geodesics and we are interested in outgoing ones. So, (4) corresponds to outgoing geodesic if the following condition is held:

$$\lim_{v\to 0\ ,r\to 0}\frac{dv}{dr}=X_0>0\ . \tag{5}$$

If the value X_0 is positive and finite, then the geodesic (4) is outgoing one. Let's consider the limit in (4):

$$X_0=\frac{2}{1-2\mu X_0}\ . \tag{6}$$

From this equation we obtain:

$$X_0^{\pm}=\frac{1\pm\sqrt{1-16\mu}}{4\mu}\ . \tag{7}$$

From this equation, one can see that in the case of the linear mass function and if $\mu<\frac{1}{16}$, then the outcome of the gravitational collapse might be the naked singularity formation. Hence, there might be particles which move away the singularity. Now we are ready to consider the front collision of two particles.

Front collision effect in the Vaidya spacetime

The Vaidya spacetime (1) is time-depended and because of it one has only one conserved quantity—the angular momentum L. In the general case, the Vaidya spacetime doesn't possess any additional symmetry. However, for the particular choice of the mass function, the metric (1) admits the conformal Killing vector (Ojako et al. 2020). In this case, M must have the following form (Nielsen 2014):

$$M\left(v\right)=\mu v,\ \mu>0\ . \tag{8}$$

Where μ is a positive constant. As we found out in the previous section, if $\mu<\frac{1}{16}$, the gravitational collapse might end with the naked singularity formation. Further in the paper we impose the condition $\mu<\frac{1}{16}$ because we are interested in the temporal naked singularity formation. If we take into account this condition and (8), then by a coordinate transformation (Solanki, Perlick 2022):

$$v=r_0e^{\frac{t}{r_0}},\quad r=Re^{\frac{t}{r_0}}\ . \tag{9}$$

one obtains the Vaidya metric in conformally static coordinates:

$$ds^2=e^{\frac{2t}{r_0}}\left[-\left(1-\frac{2\mu r_0}{R}-\frac{2R}{r_0}\right)dt^2+2dtdR+R^2d\Omega^2\right]. \tag{10}$$

We will consider the movement in the equatorial plane $\theta=\frac{\pi}{2}$. The metric (10) admits the conformal Killing vector $\frac{d}{dt}$, which is timelike in the region:

$$1-\frac{2\mu r_0}{R}-\frac{2R}{r_0}>0\ . \tag{11}$$

It means that one has the conserved energy along null geodesics in the region (11), i. e.:

$$E=e^{\frac{2t}{r_0}}\left(1-\frac{2\mu r_0}{R}-\frac{2R}{r_0}\right)\frac{dt}{d\lambda}-e^{\frac{2t}{r_0}}\frac{dR}{d\lambda}\ . \tag{12}$$

The angular momentum L has the following form:

$$L=e^{\frac{2t}{r_0}}R^2\frac{d\varphi}{d\lambda}\ . \tag{13}$$

The problem is that the energy (12) is not a constant of motion along timelike geodesics. Fortunately, the conformal Killing vector $\frac{d}{dt}$ is the homothetic Killing vector (Blau 2022) and this fact allows us to find another constant of motion along a timelike geodesic:

$$\varepsilon = E - \lambda \cdot \tag{14}$$

Despite the fact that this quantity (14) depends on the affine parameter λ, it is conserved charge along any geodesics.

To find the $\frac{dR}{d\lambda}$ component of the four velocity u^i, one should substitute (14) and (13) into the timelike condition $g_{ik}\, u^i\, u^k = -1$. Thus, one obtains:

$$e^{\frac{4t}{r_0}}\left(\frac{dR}{d\lambda}\right)^2 = E^2 - e^{\frac{2t}{r_0}}\left(1-\frac{2\mu r_0}{R}-\frac{2R}{r_0}\right)\left(\frac{L^2}{r^2 e^{\frac{2t}{r_0}}}+1\right) = e^{\frac{4t}{r_0}} P_R^2 \ . \tag{15}$$

Where $P_R = P_R\,(R,t)$ is some positive function. According to the BSW effect (Banados et al. 2009), the energy of the centre of mass $E_{c.m.}$ of the two colliding particles for the extremal Kerr black hole can grow unboundly. For this purpose, one of the particles must be a critical one (Tanatarov, Zaslavskii 2013). In the Schwarzschild spacetime, the energy $E_{c.m.}$ is finite according to the original proposal. However, if we consider, in the Schwarzschild spacetime, the collision of two particles one of which moves along the white hole geodesic from the gravitational radius and the other one moves along the black hole geodesic and falls onto the black hole (Grib, Pavlov 2015), then the energy $E_{c.m.}$ of the collision can be unbound. The problem is that the Schwarzschild metric describes the eternal black hole and the white hole geodesic appears from the region outside the white hole gravitational radius in past infinity. However, if one considers the physically relevant model, then prolonging the white hole geodesic into the past, one can see that it appears from the collapsing cloud of the matter. So, to understand this analogue of the BSW effect one, first of all, should consider the gravitational collapse model which, in the case of the Vaidya spacetime, was done in the previous section. We have proved that if $\mu < \frac{1}{16}$, the gravitational collapse might end with the naked singularity formation. For our model it means that there is a family of non-spacelike future-directed geodesics which terminate at the central singularity in the past. Let's consider the following situation: particle moves along such geodesic and when the apparent horizon forms, this particle is in the vicinity of this horizon and outside it. At this time, particle 2, which falls onto the black hole, collides with particle 1. Let's calculate if the unbounded energy $E_{c.m.}$ of the collision is possible and where this collision should take place.

For simplisity, let's consider the collision of two particles with same mass m_0. In this case, the energy $E_{c.m.}$ is given by:

$$E_{c.m.} = m_0\sqrt{2}\sqrt{1-g_{ik}u_1^i u_2^k} \ . \tag{16}$$

Where and are the four velocities of particles and respectively. Substituting (12), (13) and (15) into (16), one obtains:

$$\frac{E_{c.m.}^2}{2m_0} = 1 + \frac{E_1\left(E_2 + e^{\frac{2t}{r_0}} P_{2R}\right)}{e^{\frac{2t}{r_0}}\left(1-\frac{2\mu r_0}{R}-\frac{2R}{r_0}\right)} - \frac{e^{\frac{2t}{r_0}}\left(E_1 + e^{\frac{2t}{r_0}} P_{1R}\right)P_{2R}}{1-\frac{2\mu r_0}{R}-\frac{2R}{r_0}} - \frac{L_1 L_2}{e^{\frac{2t}{r_0}} R^2} \ . \tag{17}$$

Note that only the second and third terms in the right-hand side can give us the unbound energy $E_{c.m.}$. It is possible if:

$$1-\frac{2\mu r_0}{R_{kh}}-\frac{2R_{kh}}{r_0} = 0 \ . \tag{18}$$

 https://www.doi.org/10.33910/2687-153X-2022-4-1-17-23

Where $R = R_{kh}$ is the location of the conformal Killing horizon. Also, one should note that for outgoing particle $1 - P_{1R} > 0$, for ingoing particle $2 - P_{2R} < 0$. So, we conclude that both considered terms are positive if we consider the region (11) of the timelike conformal Killing vector $\frac{d}{dt}$ and we should prove that one of them grows unboundly when $R \to R_{kh}$. To proceed, we note that:

$$\lim_{R\to R_{kh}} e^{\frac{2t}{r_0}} P_{1R} = +E \ , \quad \lim_{R\to R_{kh}} e^{\frac{2t}{r_0}} P_{2R} = -E \ . \tag{19}$$

One should note that an off-diagonal term in the metric (10) might indicate that there are particles with negative energy. However, it was shown (Vertogradov 2020) that there are no particles with negative energy outside the apparent horizon and $E \geq 0$. Using this fact and by taking limit $R \to R_{kh}$, one can see that the second term in the right-hand side of (17) gives us uncertainty 0/0 and we won't consider it because if it is finite, then we can neglect it. If it is infinite, then we obtain the unbound $E_{c.m}$. However, we focus our attention on the third term in the right-hand side of (17):

$$\lim_{R\to R_{kh}} - \frac{e^{\frac{2t}{r_0}}\left(E_1 + e^{\frac{2t}{r_0}} P_{1R}\right) P_{2R}}{1 - \frac{2\mu r_0}{R} - \frac{2R}{r_0}} = \frac{e^{2t} r_0 2 E_1 E_2}{1 - \frac{2\mu r_0}{R} - \frac{2R}{r_0}} \to +\infty \ . \tag{20}$$

And we can see that this term (20) gives us the unbound energy $E_{c.m}$ if the collision takes place in the vicinity of the conformal Killing horizon.

Conclusions

In this paper, we have considered the front collision of two particles in the Vaidya spacetime. The metric (1) is time-depended and to consider the center-of-mass energy, one needs to introduce new coordinates which allow us to write the Vaidya spacetime in a conformally static form. It allows us to consider the following model: in the case of the linear muss function, the gravitational collapse might end up with the naked singularity. We consider the non-spacelike geodesic which originates at this naked singularity. Further, we assume that there are particles which move along this geodesic away from the central singularity. Then, the other particle falls onto a collapsing cloud and the front collision of two particles is considered at the time of the apparent horizon formation. It means that the apparent horizon forms and the particle, moving along a naked singularity geodesic, finds itself outside the trapped region, in the vicinity of the apparent horizon. We showed that the unbound center-of-mass energy is possible if the collision takes place in the vicinity of the conformal Killing horizon. Note that if we pick up the mass function as $M(v) = \mu v^n$, $n > 1$, then, of course, one has the naked singularity formation (Vertogradov 2022b). However, the singularity is gravitationally weak according to the Tipler definition (Nolan 1999; Tipler 1977) and the spacetime doesn't admit the conformal Killing vector anymore.

The unbound center-of-mass energy of the two colliding particles near the conformal Killing horizon is an expected result. One should use this horizon to define most physicaly relevant quantities. In static spacetimes, for example, one uses the Killing horizon to define the surface gravity which is associated with the Hawking temperature. The Killing horizon coinsides with the event horizon in the case of the Schwarzschild and non-extremal Reissner-Nordström black holes. However, in the dynamical case it is not an easy task to define the surface gravity (Nielsen, Yoon 2008). One can define the surface gravity on the apparent horizon but, according to Nielsen (Nielsen 2010), the apparent horizon in the Vaidya spacetime is hidden inside the event horizon, although, to define the location of the last one is also a hard task in dynamical spacetimes.

The results obtained in this paper can be easily extended to the generalized Vaidya spacetime. The naked singularity formation and the mass function conditions for this metric have been proven in (Mkenyeleye et al. 2014; Vertogradov 2016a; 2016b). The unbound center-of-mass is again expected if the front collision takes place in the vicinity of the conformal Killing horizon. However, the conformal Killing vector exists only for the following choice of the mass function:

$$M\left(v,r\right) = \mu v + \nu v^{2\alpha} r^{1-2\alpha}, \quad \mu > 0 \nu \neq 0, \quad \alpha \neq \frac{1}{2} \ . \tag{20}$$

Where $\alpha \in [-1, 1]$ (Wang, Wu 1999). Note, that for this choice of the mass function, the conformal Killing vector is the homothetic one. The generalized Vaidya spacetime admits a regular black hole solution (Hayward 2006), however, the question about the front collision in this case is still open.

Conflict of Interest

The authors declare that there is no conflict of interest, either existing or potential.

References

Banados, M., Silk, J., West, S. M. (2009) Kerr black holes as particle accelerators to arbitrarily high energy. *Physical Review Letters*, 103 (11), article 111102. https://doi.org/10.1103/PhysRevLett.103.111102 (In English)

Blau, M. (2022) *Lecture notes on general relativity*. Bern: Albert Einstein Center for Fundamental Physics Publ., 997 p. (In English)

Dey, D., Joshi, P. S., Mosani, K., Vertogradov, V. (2022) Causal structure of singularity in non-spherical gravitational collapse. *The European Physical Journal C*, 82 (5), article 431. https://doi.org/10.1140/epjc/s10052-022-10401-1 (In English)

Dwivedi, I. H., Joshi, P. S. (1989) On the nature of naked singularities in Vaidya spacetimes. *Classical and Quantum Gravity*, 6 (11), 1599 – 1606. https://doi.org/10.1088/0264-9381/6/11/013 (In English)

Grib, A. A., Pavlov, Yu. V. (2015) Are black holes totally black? *Gravitation and Cosmology*, 21 (1), 13–18. https://doi.org/10.1134/S0202289315010065 (In English)

Grib, A. A., Pavlov, Yu. V., Vertogradov, V. D. (2014) Geodesics with negative energy in the ergosphere of rotating black holes. *Modern Physics Letters A*, 29 (20), article 1450110. https://doi.org/10.1142/S0217732314501107 (In English)

Harada, T., Nemoto, H., Miyamoto, U. (2012) Upper limits of particle emission from high-energy collision and reaction near a maximally rotating Kerr black hole. *Physical Review D*, 86 (2), article 024027. https://doi.org/10.1103/PhysRevD.86.024027 (In English)

Hayward, S. A. (2006) Formation and evaporation of nonsingular black holes. *Physical Review Letters*, 96 (3), article 031103. https://doi.org/10.1103/PhysRevLett.96.031103 (In English)

Joshi, P. S. (2007) *Gravitational collapse and spacetime singularities*. New York: Cambridge University Press, 273 p. https://doi.org/10.1017/CBO9780511536274 (In English)

Joshi, P. S., Malafarina, D. (2011) Recent developments in gravitational collapse and spacetime singularities. *International Journal of Modern Physics D*, 20 (14), 2641–2729. https://doi.org/10.1142/S0218271811020792 (In English)

Mkenyeleye, M. D., Goswami, R., Maharaj, S. D. (2014) Gravitational collapse of generalized Vaidya spacetime. *Physical Review D*, 90 (6), article 064034. https://doi.org/10.1103/PhysRevD.90.064034 (In English)

Nielsen, A. B. (2010) The spatial relation between the event horizon and trapping horizon. *Classical and Quantum Gravity*, 27 (24), article 245016. https://doi.org/10.1088/0264-9381/27/24/245016 (In English)

Nielsen, A. B. (2014) Revisiting vaidya horizons. *Galaxies*, 2 (1), 62–71. https://doi.org/10.3390/galaxies2010062 (In English)

Nielsen, A. B., Yoon, J.-H. (2008) Dynamical surface gravity. *Classical and Quantum Gravity*, 25 (8), article 085010. https://doi.org/10.1088/0264-9381/25/8/085010 (In English)

Nolan, B. C. (1999) Strengths of singularities in spherical symmetry. *Physical Review D*, 60 (2), article 024014. https://doi.org/10.1103/PhysRevD.60.024014 (In English)

Ojako, S., Goswami, R., Maharaj, S. D., Narain, R. (2020) Conformal symmetries in generalised Vaidya spacetimes. *Classical and Quantum Gravity*, 37 (5), article 055005. https://doi.org/10.1088/1361-6382/ab5e2d (In English)

Papapetrou, A. (1985) *A Random Walk in Relativity and Cosmology*. New Delhi: Wiley Eastern Publ., 236 p. (In English)

Poisson, E. (2004) *A relativist's toolkit: The mathematics of black-hole mechanics*. Cambridge: Cambridge University Press, 233 p. (In English)

Solanki, J., Perlick, V. (2022) Photon sphere and shadow of a time-dependent black hole described by a Vaidya metric. *Physical Review D*, 105 (6), article 064056. https://doi.org/10.1103/PhysRevD.105.064056 (In English)

Tanatarov, I. V., Zaslavskii, O. B. (2013) Banados-Silk-West effect with nongeodesic particles: Extremal horizons. *Physical Review D*, 88 (6), article 064036. https://doi.org/10.1103/PhysRevD.88.064036 (In English)

Tipler, F. J. (1977) Singularities in conformally flat spacetimes. *Physics Letters A*, 64 (1), 8–10. https://doi.org/10.1016/0375-9601(77)90508-4 (In English)

Vaidya, P. C. (1951) Nonstatic solutions of Einstein's field equations for spheres of fluids radiating energy. *Physical Review*, 83 (1), article 10. https://doi.org/10.1103/PhysRev.83.10 (In English)

Vertogradov, V. D. (2015) Geodesics for particles with negative energy in Kerr's metric. *Gravitation and Cosmology*, 21 (2), 171–174. https://doi.org/10.1134/S0202289315020115 (In English)

Vertogradov, V. D. (2016a) Naked singularity formation in generalized Vaidya space-time. *Gravitation and Cosmology*, 22 (2), 220–223. https://doi.org/10.1134/S020228931602016X (In English)
Vertogradov, V. D. (2016b) Gravitational collapse of Vaidya spacetime. *International Journal of Modern Physics: Conference Series*, 41, article 1660124. https://doi.org/10.1142/S2010194516601241 (In English)
Vertogradov, V. D. (2018) The eternal naked singularity formation in the case of gravitational collapse of generalized Vaidya space–time. *International Journal of Modern Physics A*, 33 (17), article 1850102. https://doi.org/10.1142/S0217751X18501026 (In English)
Vertogradov, V. D. (2020) The negative energy in generalized vaidya spacetime. *Universe*, 6 (9), article 155. https://doi.org/10.3390/universe6090155 (In English)
Vertogradov, V. D. (2021) The nature of the naked singularity in generalized Vaidya spacetime and white hole geodesics. *Physics of Complex Systems*, 2 (1), 33–40. https://doi.org/10.33910/2687-153X-2021-2-1-33-40 (In English)
Vertogradov, V. D. (2022a) The structure of the generalized Vaidya spacetime containing the eternal naked singularity. *International Journal of Modern Physics A*, vol. 37, no. 28n29, article 2250185. https://doi.org/10.1142/S0217751X22501858 (In English)
Vertogradov, V. D. (2022b) Non-linearity of Vaidya spacetime and forces in the central naked singularity. *Physics of Complex Systems*, 3 (2), 81–85. https://doi.org/10.33910/2687-153X-2022-3-2-81-85 (In English)
Wang, A., Wu, Y. (1999) Generalized vaidya solutions. *General Relativity and Gravitation*, 31 (1), 107–114. https://doi.org/10.1023/A:1018819521971 (In English)
Zaslavskii, O. B. (2012a). Acceleration of particles by black holes as a result of deceleration: Ultimate manifestation of kinematic nature of BSW effect. *Physics Letters B*, 712 (3), 161–164. https://doi.org/10.1016/j.physletb.2012.05.009 (In English)
Zaslavskii, O. B. (2012b) Energy extraction from extremal charged black holes due to the Banados-Silk-West effect. *Physical Review D*, 86 (12), article 124039. https://doi.org/10.1103/PhysRevD.86.124039 (In English)

Theoretical physics.
Physics of atoms and molecules

UDC 539.1

EDN KCPGCI
https://www.doi.org/10.33910/2687-153X-2022-4-1-24-29

On mutual neutralization process in collisions of magnesium with hydrogen isotopes

Ya. V. Voronov[1], A. K. Belyaev✉[1]

[1] Herzen State Pedagogical University of Russia, 48 Moika Emb., Saint Petersburg 191186, Russia

Authors

Yaroslav V. Voronov, ORCID: 0000-0002-4377-7827, e-mail: voronovj@herzen.spb.ru

Andrey K. Belyaev, ORCID: 0000-0001-8834-1456, e-mail: akbelyaev@herzen.spb.ru

For citation: Voronov, Ya. V., Belyaev, A. K. (2023) On mutual neutralization process in collisions of magnesium with hydrogen isotopes. *Physics of Complex Systems*, 4 (1), 24–29. https://www.doi.org/10.33910/2687-153X-2022-4-1-24-29 EDN KCPGCI

Received 19 December 2022; reviewed 18 January 2023; accepted 18 January 2023.

Funding: Authors gratefully acknowledge support from the Ministry of Education (the Russian Federation), Project No. FSZN-2020-0026.

Abstract. Cross sections for mutual neutralization processes in magnesium-deuterium collisions are calculated in the collision energy range 0.001–100 eV by the probability current method. Special attention is given to the collision energies in the vicinity of E_{col} = 0.059 eV. Partial rate coefficients for mutual neutralization processes are calculated at the temperature T = 6000 K and compared with previous experimental and theoretical results. It is shown that the present data agree reasonably with the previous results.

Keywords: atomic data, atomic processes, charge transfer, magnesium, mutual neutralization

Introduction

Magnesium-hydrogen inelastic collisions have been intensively investigated theoretically (see Barklem 2016; 2017; Belyaev et al. 2012; Guitou et al. 2015; Rodionov, Belyaev 2017) but not experimentally. Recently, Grumer et. al. (Grumer et. al. 2022) have reported experimental measurements of the mutual neutralization (MN) cross sections in $Mg^+ + D^-$ collisions and theoretical estimates obtained by the Linear Combination of Atomic Orbitals (LCAO) method and the multichannel Landau-Zener (LZ) model approach. They claimed they got better agreement of their model estimates with the experimental data than the full quantum (FQ) theoretical data (Belyaev et al. 2012) for the final-state branching fractions (BF) and concluded that the model approach describes inelastic collision processes better than the FQ theory. For this reason in this paper we perform the new model calculations for $Mg^+ + H^-/D^-$ collisions, analyze MN BFs obtained by different theoretical means, and discuss some conclusions of (Grumer et al. 2022) with which we disagree.

Analysis of $Mg^+ + H^-/D^-$ branching fractions of mutual neutralization processes

We performed the nonadiabatic nuclear dynamical calculation for the mutual neutralization process in $Mg^+ + H^-/D^-$ collisions within the $^2\Sigma^+$ molecular symmetry based on the most recent *ab initio* data from (Guitou et al. 2015) by two model LZ approaches: the probability current method (PC) and the multichannel formula. BFs are investigated for the collision energy in the vicinity of E_{col} = 0.059 eV. Both methods treat 9 *ab initio* potential energy curves and one additional model potential, which corresponds to the Mg(3s4p ^{1}P) + H(1s ^{2}S) scattering channel, obtained by the asymptotic method (Belyaev 2013).

This state is added because both the simplified model (Belyaev, Yakovleva 2017a; 2017b) and the recent experiment (Grumer et al. 2022) indicate that the scattering channel Mg(3s4p ^{1}P) + H(1s ^{2}S) has non-negligible contribution into the total cross section and rate coefficient, so this state should be treated in nuclear dynamical calculations. The asymptotic energy for the Mg(3s4p ^{1}P) + H(1s ^{2}S) state is taken from NIST database (Kramida et al. 2022). In addition, the MgH fine structure is taken into account for multichannel calculations by means of the approach recently derived in (Belyaev et al. 2019; Yakovleva et al. 2019).

The present results are collected in Table 1 together with the data from (Guitou et al. 2015) and (Grumer et al. 2022). Fig. 1 shows the branching fractions for the mutual neutralization processes $Mg^+ + H^-/D^- \rightarrow Mg^*(3s\,nl) + H/D$ into the magnesium final states Mg(3s4s ^{3}S), Mg(3s4s ^{1}S), Mg(3s3d ^{1}D), and for a sum of the indistinguishable states (Mg(3s4p ^{3}P^o) + Mg(3s3d ^{3}D)).

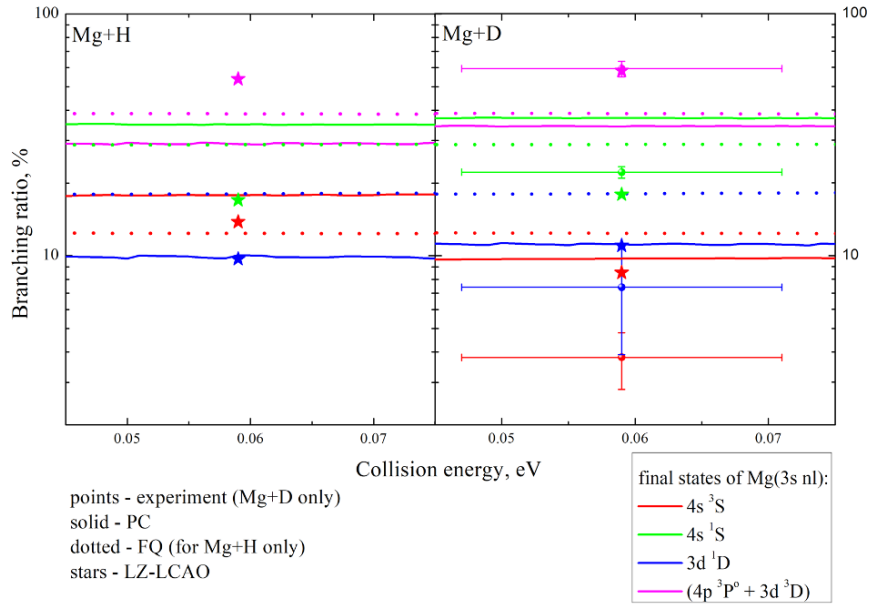

Fig. 1. Branching fractions (in per cents) of mutual neutralization processes $Mg^+ + H^-/D^- \rightarrow Mg^*(3s\,nl) + H/D$. Points with error bars correspond to the experiment (Grumer et al. 2022), stars—to the theoretical estimates of (Grumer et al. 2022), solid lines—to the Probability Current results obtained in the present work, dotted lines—to the Full Quantum results (Guitou et al. 2015)

Table 1. Mutual neutralization branching fractions (in per cent) calculated from the cross sections obtained by different means. (1) (Guitou et al. 2015), (2) (Grumer et al. 2022), (3) present calculations. Columns 2–5 correspond to $Mg^+ + H^-$ collisions, columns 6–9 correspond to $Mg^+ + D^-$ collisions

	FQ[1]	LZ-LCAO[2]	PC[3]	LZ-fine structure[3]	LZ-LCAO[2]	Experiment[2]	PC[3]	LZ-fine structure[3]
Mg final state	H^-	H^-	H^-	H^-	D^-	D^-	D^-	D^-
3s^2 ^{1}S	0.0	0.0	0.00	0.00	0.0	–	0.00	0.00
3s3p ^{3}P	0.0	0.0	0.00	0.00	0.0	–	0.00	0.00
3s3p ^{1}P	1.5	3.1	3.17	1.82	1.1	0.4 ± 0.1	1.33	0.41
3s4s ^{3}S	14.8	13.8	18.03	17.59	8.5	3.8 ± 1.0	9.86	8.91
3s4s ^{1}S	29.3	17.0	35.65	35.16	17.9	22.1 ± 1.2	37.30	36.56
3s3d ^{1}D	6.9	9.7	9.28	8.39	11.0	7.4 ± 3.5	10.82	10.01
3s4p ^{3}P	20.5	33.5	17.40	16.93	33.7	59.2 ± 4.4	20.41	19.87
3s3d ^{3}D	22.3	20.3	11.20	11.17	24.4		13.74	13.36
3s4p ^{1}P	4.4	2.5	5.27	8.93	3.4	7.1 ± 1.0	6.54	10.88
3s5s ^{3}S	0.2	0.0	–	–	0.0	–	–	–
3s5s ^{1}S	0.2	0.0	–	–	0.0	–	–	–

Let us consider magnesium-deuterium collisions. From the right panel of Fig. 1 it is seen that all considered methods provide results in very good agreement to each other for the magnesium final states Mg(3s4s ^{3}S) and Mg(3s3d ^{1}D) (red and blue lines and symbols), but for the states Mg(3s4s ^{1}S) and (Mg(3s4p ^{3}P^o) + Mg(3s3d ^{3}D)) there exists a difference between experimental and LZ-LCAO data as well as between the data obtained by the FQ and PC methods. It is clearly seen from Table 1 that the largest BFs correspond to the states Mg(3s4s ^{1}S), Mg(3s4p ^{3}P) and Mg(3s3d ^{3}D). The total BFs summed over these three states are 76% (LZ-LCAO), 81.3 ± 5.6% (experiment), 71.45% (PC) and 69.79% (LZ-fine structure). The LZ-LCAO results agree the best with the experiment, although the results of PC and LZ-fine-structure calculations are also in good agreement with the experiment. It also should be noted that the general behavior of all BFs is in good agreement with each other for all sets of data, and the experimentally observed final-state distribution is correctly reproduced by the different theoretical approaches.

Let us consider magnesium-hydrogen collisions. For this system, to the best of our knowledge, there are no experimental data, but FQ data are available. There are four final states with the largest BFs values: Mg(3s4s ^{3}S), Mg(3s4s ^{1}S), Mg(3s4p ^{3}P) and Mg(3s3d ^{3}D), and the total BFs for these four states are: 86.9% (FQ), 84.6% (LZ-LCAO), 82.28% (PC) and 80.85% (LZ-fine structure). These results are in good agreement with each other as well, and again the general behavior of all BFs is in reasonable agreement with the FQ one, see the left panel of Fig. 1. FQ and PC methods predict that MN BF into the final state Mg(3s4s ^{1}S) is larger than the LZ-LCAO estimates by a factor of 2, but BF into the states (Mg(3s4p ^{3}P^o) + Mg(3s3d ^{3}D)) is lower than the LZ-LCAO estimates also by a factor of 2. It is worth noting that all data-sets are in reasonable agreement with each other.

Since the only difference between the $Mg^+ + H^-$ and $Mg^+ + D^-$ collisions is in masses of a hydrogen isotope, it is expected that in both cases BF distributions are similar; this has been confirmed theoretically and experimentally for LiH (Belyaev, Voronov 2021; Launoy et al. 2019; Schmidt-May et al. 2022). Theoretical calculations for the $Mg^+ + H^-$ and $Mg^+ + D^-$ collisions confirm this conclusion, see Table 1.

Analysis of $Mg^+ + H^-$ rate coefficients of mutual neutralization processes

Let us now discuss the rate coefficients obtained by different theoretical methods. Table 2 contains the rate coefficients for Mg+H collisions obtained by FQ calculations, LZ-LCAO calculations from (Barklem 2017; 2022), LZ-LCAO calculations from (Grumer et al. 2022), PC and LZ-fine structure (the present study).

Table 2. Mutual neutralization rate coefficients of $Mg^+ + H^-$ collisions at the temperature T = 6000 K calculated from the cross sections obtained by different means. (1) (Guitou et al. 2015), (2) Barklem 2022, (3) (Grumer et al. 2022), (4) present calculations. Square brackets denote the power of ten.

Mg final state	FQ[1]	LZ-LCAO[2] (.rates)	LZ-LCAO[2] (.min)	LZ-LCAO[2] (.max)	LZ-LCAO[3]	PC[4]	LZ-fine structure[4]
3s^2 ^{1}S	1.44[–12]	0	0	1.48[–14]	–	1.49[–18]	5.49[–19]
3s3p ^{3}P	1.01[–9]	5.49[–12]	6.74[–22]	1.51[–11]	–	4.11[–15]	4.82[–13]
3s3p ^{1}P	4.00[–9]	5.14[–9]	1.13[–12]	5.14[–9]	–	4.62[–9]	2.95[–9]
3s4s ^{3}S	2.00[–8]	2.23[–8]	1.27[–10]	2.23[–8]	–	2.60[–8]	2.39[–8]
3s4s ^{1}S	4.18[–8]	2.64[–8]	2.64[–8]	3.99[–8]	–	3.93[–8]	3.87[–8]
3s3d ^{1}D	2.58[–8]	1.57[–8]	9.46[–9]	5.12[–8]	–	1.20[–8]	9.40[–9]
3s4p ^{3}P	2.01[–8]	5.45[–8]	2.65[–8]	6.94[–8]	–	1.95[–8]	1.92[–8]
3s3d ^{3}D	3.16[–8]	3.36[–8]	1.36[–8]	3.36[–8]	–	1.50[–8]	1.25[–8]
3s4p ^{1}P	5.62[–9]	3.94[–9]	3.94[–9]	1.04[–8]	–	6.27[–9]	5.92[–9]
3s5s ^{3}S	3.06[–10]	8.03[–12]	4.95[–12]	1.95[–11]	–	–	–
3s5s ^{1}S	3.23[–10]	3.38[–14]	3.38[–14]	2.61[–13]	–	–	–
total	1.5[–7]	1.6[–7]	0.8[–7]	2.3[–7]	1.6[–7]	1.2[–7]	1.1[–7]

 https://www.doi.org/10.33910/2687-153X-2022-4-1-24-29

It should be noted that in the LZ-LCAO calculations the "fluctuations" of rate coefficients can be significant, for example, the scatter of the total rate coefficient is equal to (0.8-2.3) x 10^{-7} cm^3/s. For partial processes these "fluctuations" may exceed several orders of magnitude.

Let us analyze the data from the columns 2, 3, 6–8 in detail. One can see from Table 2 that the total MN rate coefficient obtained by different methods has values in the range (1.1-1.6) x 10^{-7} cm^3/s and agrees within the uncertainty ≈30% with the FQ data (1.5 x 10^{-7} cm^3/s).

The MN processes into the final magnesium states Mg(3s4s ^{3}S), Mg(3s4s ^{1}S), Mg(3s3d ^{1}D), Mg(3s4p ^{3}P), Mg(3s3d ^{3}D), Mg(3s4p ^{1}P) are of particular interest because these processes belong to the so-called "optimal window" according to the simplified model (Belyaev, Yakovleva 2017a; 2017b). The optimal window for Mg is located at the excitation energy range of 5.1–6.1 eV. Table 2 shows that the main deviations of our present results from those of the FQ and LZ-LCAO results are for the processes $Mg^+ + H^- \rightarrow$ Mg(3s4s ^{1}S) + H(1s ^{2}S), Mg(3s4p ^{3}P) + H(1s ^{2}S), Mg(3s3d ^{3}D) + H(1s ^{2}S). These differences do not exceed the factor of 3, which is less than almost all "fluctuation" ranges for these processes obtained by LZ-LCAO method (columns 4–5). In general, we conclude that the MN rate coefficients with the values exceeding 10^{-8} cm^3/s and obtained by different theoretical methods agree reasonably well with each other.

Discussion

Let us discuss some conclusions from (Grumer et al. 2022). First of all, it should be noted that Grumer et.al. (Grumer et al. 2022) compared their results with FQ results from (Belyaev et al. 2012), which is not the most recent work and does not include the most complete FQ data. The most recent MgH treatment was reported in the (Guitou et al. 2015) paper for 13 MgH states, while in the (Belyaev et al. 2012) paper only eight states of the MgH molecule were considered: seven covalent and one ionic states. The comparison of the truncated data from the (Belyaev et al. 2012) paper instead of the complete data (Guitou et al. 2015) with the experimental and theoretical data (Grumer et al. 2022) misleaded Grumer et al. to the wrong conclusions. Namely:

1) (Grumer et al. 2022) wrote, "The FQ for Mg+H calculation, with Mg(4s ^{1}S) as the predicted dominating channel with a branching fraction of 61.9%, reproduces the experimental data poorly. The current state-of-the-art theoretical data, based on detailed quantum-chemistry calculations, do not correctly reproduce the observed final-state distributions."

Grumer et al. (Grumer et al. 2022) made such conclusion because they compared their theoretical and experimental data for 11 scattering final channels in Mg+H and Mg+D collisions with the data calculated for seven final scattering channels (Belyaev et al. 2012) in Mg+H collisions. In this case, one or two of the most populated final channels were not included into the consideration. Grumer et al. (Grumer et al. 2022) obtained the BF of 61.9% for the Mg(3s4s ^{1}S) + H final state by taking into calculation only the truncated data set of seven final covalent channels from (Belyaev et al. 2012) while for their calculations of the BFs by the LZ-LCAO method Grumer et. al. (Grumer et al. 2022) took into account 11 final covalent channels. This leads to the BFs of 17.0% (Mg+H) and 17.9% (Mg+D) as well as to the experimental value of 22.1%±1.2%. Obviously, the BF distribution depends on a number of scattering channels taken into calculations, and the most accurate state-of-the-art theoretical FQ data were presented in (Guitou et al. 2015) for 13 molecular states. It is shown in the previous section that FQ as well as PC and LZ-fine structure methods based on the *ab initio* potentials provide the results that are in reasonable agreement with the experimental data: in Mg+H collisions BFs for magnesium state Mg(3s4s ^{1}S) is 29.3% for FQ, 35.65% for PC and 35.16% for LZ-fine structure method. Thus, the conclusion (1) is incorrect. The correct calculations of the complete FQ data lead to a good agreement with the experimental data.

2) Grumer et al. wrote, "Asymptotic model calculations are shown to describe the process much better (than FQ)" (Grumer et al. 2022).

The LCAO method should be compared with the *ab initio* Multi-Reference Configuration Interaction (MRCI) method used in (Guitou et al. 2015). Calculations performed by Guitou et al. (Guitou et al. 2015) were based on 57 basis orbitals for Mg plus 23 basis orbitals for H plus 5 diffuse orbitals, that is, 85 basis wavefunctions as a starting point in total. The LCAO method used a single undisturbed orbital for H^- and a few orbitals for covalent states. Obviously, the MRCI calculations are more accurate than those by the LCAO used in (Grumer et al. 2022). So, the conclusion (2) is also wrong.

3) Grumer et al. wrote, "A simpler asymptotic-model approach based on multichannel Landau-Zener dynamics combined with a LCAO approach for the coupling strengths describes the MN process and the resulting excitations of the neutral products much better (than FQ)" (Grumer et al. 2022).

There are several arguments to contradict this statement:

a) when the electronic structure, potentials and couplings are known with high accuracy over the whole range of internuclear configurations, the accurate non-adiabatic nuclear dynamics can be calculated by solving the Coupled Channel Equations (CCEs) taken into account not only long-range but also intermediate- and short-range non-adiabatic regions as well as all non-adiabatic couplings. This is done in (Guitou et al. 2015) and also in the present investigation by the PC method within the LZ model. Alternatively, the multichannel analytical formula can be used for estimate state-to-state transition probabilities, when non-adiabatic regions are localized in a particular sequence, usually for long- and intermediate-range regions; short-range regions are usually not taken into account in this kind of estimates. Grumer et al. (Grumer et al. 2022) used the multichannel formula. Obviously, solutions of the CCEs have higher accuracy than the multichannel formula, though the latter has some advantages.

b) In the collision theory there is the fundamental problem, the so-called Electron Translation (ET) problem (sometimes called the Molecular-state problem), related to non-zero asymptotic non-adiabatic radial couplings. It is shown in (Belyaev 2010) that this might lead to divergence of a partial cross section. Guitou et al. (Guitou et al. 2015) solved the ET problem by using the reprojection method (Belyaev 2010; Grosser et al. 1999), while Grumer et al. (Grumer et al. 2022) did not take this problem into account. Thus, FQ (full quantum) non-adiabatic nuclear dynamical treatment is more complete and more accurate than the multichannel approach, and the conclusion (3) of the paper (Grumer et al. 2022) is also not correct.

Finally, we come to the general conclusion that the FQ study of inelastic collision processes, in particular, the FQ of MN in $Mg^+ + H^-/D^-$ collisions, is more accurate than the model estimates of (Grumer et al. 2022). However, we wish to point out that FQ calculations are time-consuming and expensive, and hence model approaches are useful and efficient.

In the case of magnesium-hydrogen collisions, we believe that new accurate quantum-chemical calculations of the adiabatic potentials and couplings are desired, in particular, taking into account more excited MgH molecular states, at least $Mg(3s4p\ ^1P^o) + H(1s\ ^2S)$.

Conclusions

In this work, we investigated the mutual neutralization processes in collisions of $Mg^+ + H^-/D^-$ at the vicinity of the collision energy E_{col} = 0.059 eV by the probability current method and by the multichannel formula (with accounting for fine structure). It is shown that the results based on the ab initio potential energy curves from (Guitou et al. 2015) have reasonable agreement with the full quantum nuclear dynamical calculations (Guitou et al. 2015), with the LCAO-multichannel-LZ estimates (Grumer et al. 2022), and with the experimental data (Grumer et al. 2022). We emphasize that new quantum-chemical calculations of the adiabatic potentials and couplings taking into account higher-lying excited MgH molecular states, at least $Mg(3s4p\ ^1P^o) + H(1s\ ^2S)$, are highly desired.

Conflict of Interest

The authors declare that there is no conflict of interest, either existing or potential.

Author Contributions

The authors have made an equal contribution to the paper.

Acknowledgements

The authors gratefully thank Prof. Nicole Feautrier and Dr. Alexander Mitrushchenkov for fruitful discussions.

References

Barklem, P. S. (2016) Excitation and charge transfer in low-energy hydrogen-atom collisions with neutral atoms: Theory, comparisons, and application to Ca. *Physical Review A*, 93 (4), article 042705. https://doi.org/10.1103/PhysRevA.93.042705 (In English)

Barklem, P. S. (2017) Erratum: Excitation and charge transfer in low-energy hydrogen-atom collisions with neutral atoms: Theory, comparisons, and application to Ca [Phys. Rev. A 93, 042705 (2016)]. *Physical Review A*, 95(6), article 069906(E). https://doi.org/10.1103/PhysRevA.95.069906 (In English)

Barklem, P. S. (2022) Public-data. *Github.* [Online]. Available at: https://github.com/barklem/public-data (accessed 01.11.2022). (In English)

Belyaev, A. K. (2010) Revised Born-Oppenheimer approach and a reprojection method for inelastic collisions. *Physical Review A*, 82 (6), article 060701. https://doi.org/10.1103/PhysRevA.82.060701 (In English)

Belyaev, A. K. (2013) Model approach for low-energy inelastic atomic collisions and application to Al + H and $Al^+ + H^-$. *Physical Review A*, 88 (5), article 052704. https://doi.org/10.1103/PhysRevA.88.052704 (In English)

Belyaev, A. K. Barklem, P. S., Spielfiedel, A. et. al. (2012) Cross sections for low-energy inelastic Mg + H and $Mg^+ + H^-$ collisions. *Physical Review A*, 85 (3), article 032704. https://doi.org/10.1103/PhysRevA.85.032704 (In English)

Belyaev, A. K., Voronov, Ya. V. (2021) Isotopic effects in low-energy lithium-hydrogen collisions. *Physical Review A*, 104 (2), article 022812. https://doi.org/10.1103/PhysRevA.104.022812 (In English)

Belyaev, A. K., Voronov, Ya. V., Yakovleva, S. A. (2019) Inelastic processes in calcium-hydrogen ionic collisions with account for fine structure. *Physical Review A*, 100 (6), article 062710. https://doi.org/10.1103/PhysRevA.100.062710 (In English)

Belyaev, A. K., Yakovleva, S. A. (2017a). Estimating inelastic heavy-particle–hydrogen collision data-I. Simplified model and application to potassium-hydrogen collisions. *Astronomy & Astrophysics*, 606, article A147. https://doi.org/10.1051/0004-6361/201731015 (In English)

Belyaev, A. K., Yakovleva, S. A. (2017b). Estimating inelastic heavy-particle–hydrogen collision data-II. Simplified model for ionic collisions and application to barium-hydrogen ionic collisions. *Astronomy & Astrophysics*, 608, article A33. https://doi.org/10.1051/0004-6361/201731882 (In English)

Grosser, J., Menzel, T., Belyaev, A. K. (1999) Approach to electron translation in low-energy atomic collisions. *Physical Review A*, 59 (2), article 1309. https://doi.org/10.1103/PhysRevA.59.1309 (In English)

Grumer, J., Eklund, G., Amarsi, A. M. et. al. (2022) State-resolved mutual neutralization of Mg^+ and D^-. *Physical Review Letters*, 128 (3), article 033401. https://doi.org/10.1103/PhysRevLett.128.033401 (In English)

Guitou, M., Spielfiedel, A., Rodionov, D. S. et.al. (2015) Quantum chemistry and nuclear dynamics as diagnostic tools for stellar atmosphere modeling. *Chemical Physics*, 462, 94–103. https://doi.org/10.1016/j.chemphys.2015.06.003 (In English)

Kramida, A., Ralchenko, Yu., Reader, J. (2022) *Atomic Spectra Database. NIST Standard Reference Database 78 (version 5.10)*. [Online]. Available at: https://doi.org/10.18434/T4W30F (accessed 05.12.2022). (In English)

Launoy, T., Loreau, J., Dochain, A. et. al. (2019) Mutual neutralization in $Li^+ – D^-$ collisions: A combined experimental and theoretical study. *The Astrophysical Journal*, 883 (1), article 85. https://doi.org/10.3847/1538-4357/ab3346 (In English)

Rodionov, D. S., Belyaev, A. K. (2017) Low-energy inelastic atomic collisions of magnesium and hydrogen. *Russian Journal of Physical Chemistry B*, 11 (1), 34–36. https://doi.org/10.1134/S1990793117010304

Schmidt-May, A. F., Eklund, G., Rosén, S. et. al. (2022) Experimental confirmation of the isotope effect on the branching in mutual neutralization. In: *Proceedings of the DESIREE Symposium 2022 (22–24 August, 2022)*. Stockholm: Stockholm University Publ., p. 23. (In English)

Yakovleva, S. A., Voronov, Ya. V., Belyaev, A. K. (2019) The fine structure of alkali metal atoms in inelastic collisions with hydrogen. *Optics and Spectroscopy*, 127 (2), 207–211. https://doi.org/10.1134/S0030400X19080289 (In English)

Physics of Semiconductors. Physics of thin films

UDC 538.9

EDN KJGEWB
https://www.doi.org/10.33910/2687-153X-2022-4-1-30-35

Local environment of germanium atoms in $Ge_3Sb_2Te_6$, $Ge_2Sb_2Te_5$, $GeSb_2Te_4$ and $GeSb_4Te_7$ amorphous and crystalline films

Yu. A. Petrushin✉[1]

[1] Herzen State Pedagogical University of Russia, 48 Moika Emb., Saint Petersburg 191186, Russia

Author
Yuri A. Petrushin, ORCID: 0000-0002-9873-2685, e-mail: uraordie@mail.ru

For citation: Petrushin, Yu. A. (2023) Local environment of germanium atoms in $Ge_3Sb_2Te_6$, $Ge_2Sb_2Te_5$, $GeSb_2Te_4$ and $GeSb_4Te_7$ amorphous and crystalline films. *Physics of Complex Systems*, 4 (1), 30–35. https://www.doi.org/10.33910/2687-153X-2022-4-1-30-35 EDN KJGEWB

Received 13 December 2022; reviewed 18 January 2023; accepted 18 January 2023.

Funding: The study did not receive any external funding.

Abstract. The valence state and local environment of germanium atoms in $Ge_3Sb_2Te_6$, $Ge_2Sb_2Te_5$, $GeSb_2Te_4$ and $GeSb_4Te_7$ amorphous and crystalline films were determined by Mössbauer spectroscopy on the ^{119}Sn isotope. In crystalline films, divalent germanium is located in octahedral positions in a rhombohedrally distorted NaCl-type crystal lattice. In amorphous films, tetravalent germanium atoms form a tetrahedral system of chemical bonds. In all the films, the nearest environment of germanium contains mainly tellurium atoms.

Keywords: local structure, Mössbauer spectroscopy, amorphous and crystalline films, valence state, local environment

Introduction

Due to a significant contrast in conductivity and reflectivity between the crystalline and amorphous phases, phase transition materials can be used to store and encode data for non-volatile memory (Lencer et al. 2011). It is believed that the compositions lying on the GeTe–Sb_2Te_3 pseudobinary line ($Ge_3Sb_2Te_6$, $Ge_2Sb_2Te_5$, $GeSb_2Te_4$ and $GeSb_4Te_7$, let us denote them as GeSbTe) are the most promising materials for creating rewritable optical storage devices, since they have a short crystallization time, ideal reversibility between amorphous and crystalline states and high thermal stability (Qiao et al. 2019). To date, the crystal structures of GeSbTe alloys (let us denote them as *c*-GeSbTe) have been studied in detail (Lotnyk et al. 2016; Sun et al. 2007; Urban et al. 2013; Wang et al. 2017; Zhang et al. 2016; Zheng et al. 2019). Many studies have also been carried out in order to determine the short-range structure of GeSbTe amorphous alloys (let us denote them as *a*-GeSbTe) (Baker et al. 2006; Jóvári et al. 2008; Kolobov et al. 2004; Paesler et al. 2007); however, these structures are still being discussed (Qiao et al. 2019; Stellhorn et al. 2020).

Mössbauer spectroscopy (MS) can be an effective tool for changes detecting in the local environment of atoms and their electronic structure during GeSbTe compounds amorphization. However, apart from the works (Bordovskii et al. 2021; Marchenko et al. 2021) and the work (Ledda et al. 1988), which presents the ^{121}Sb Mössbauer spectra of $GeSb_2Te_4$, $Ge_2Sb_2Te_5$ and $GeSb_4Te_7$ crystalline compounds, there are no Mössbauer studies of GeSbTe ternary compounds.

This work is devoted to studying the nature of the local environment of germanium atoms in $Ge_3Sb_2Te_6$, $Ge_2Sb_2Te_5$, $GeSb_2Te_4$ and $GeSb_4Te_7$ crystalline and amorphous films by absorption MS on ^{119}Sn isotope.

Experimental technique

Undoped and tin-doped X-ray $Ge_3Sb_2Te_6$, $Ge_2Sb_2Te_5$, $GeSb_2Te_4$, $GeSb_4Te_7$, $Ge_{2.95}Sn_{0.05}Sb_2Te_6$, $Ge_{1.95}Sn_{0.05}Sb_2Te_5$, $Ge_{0.95}Sn_{0.05}Sb_2Te_4$ and $Ge_{1.95}Sn_{0.05}GeSb_4Te_4$ amorphous films (let us denote them as *a*-Ge(Sn)SbTe) were obtained by magnetron sputtering of polycrystalline targets. The films were annealed at 150 °C to obtain GeSbTe and Ge(Sn)SbTe crystalline films. The films composition was monitored by the X-ray fluorescence analysis.

The Mössbauer spectra were measured with a SM 4201 TerLab spectrometer at 80 K using a $Ca^{119mm}SnO$ source. Isomer shifts (δ) of the ^{119}Sn spectra are given relative to the $CaSnO_3$ absorber.

Experimental results and their discussion

The Mössbauer spectra of ^{119}Sn impurity atoms in Ge(Sn)SbTe amorphous and crystalline films are shown in Figs. 1 and 2. All spectra are single lines with a FWHM G ~ 1.30–1.36 mm/s. (The instrumental line width G_{app} = 0.79(2) mm/s). The crystalline films spectra have isomer shifts δ ~ 3.49–3.54 mm/s; for amorphous films δ ~ 2.03–2.09 mm/s was obtained.

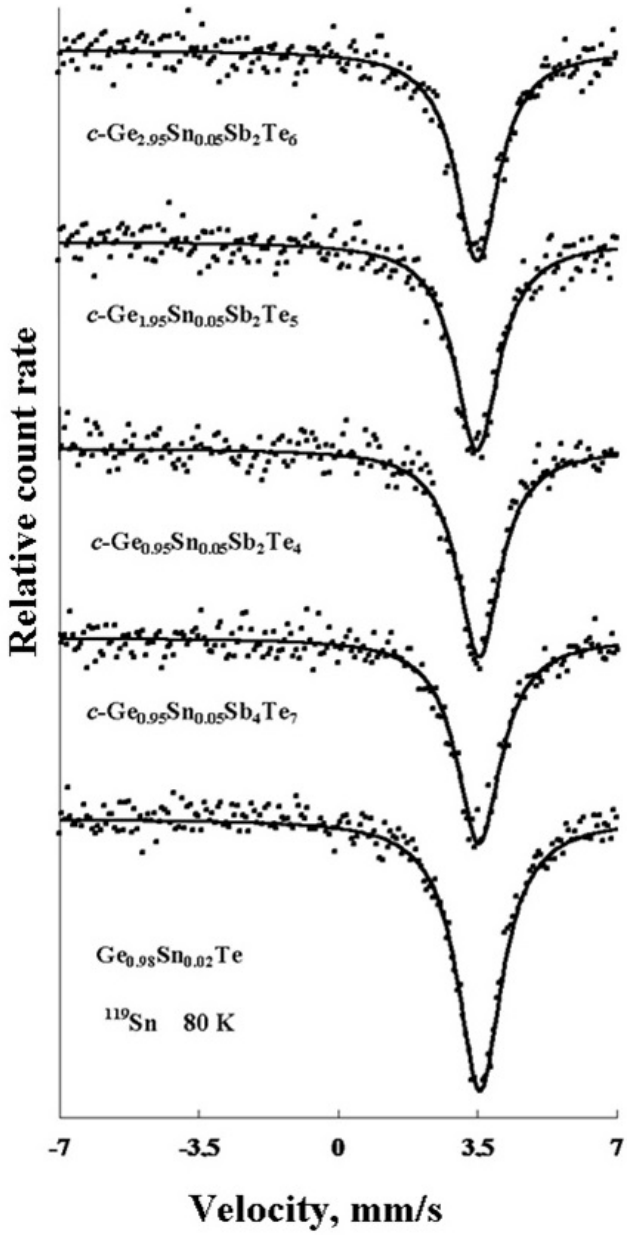

Fig. 1. Mössbauer spectra of ^{119}Sn impurity atoms in Ge(Sn)Sb crystalline films and in the $Ge_{0.98}Sn_{0.02}Te$ crystalline compound

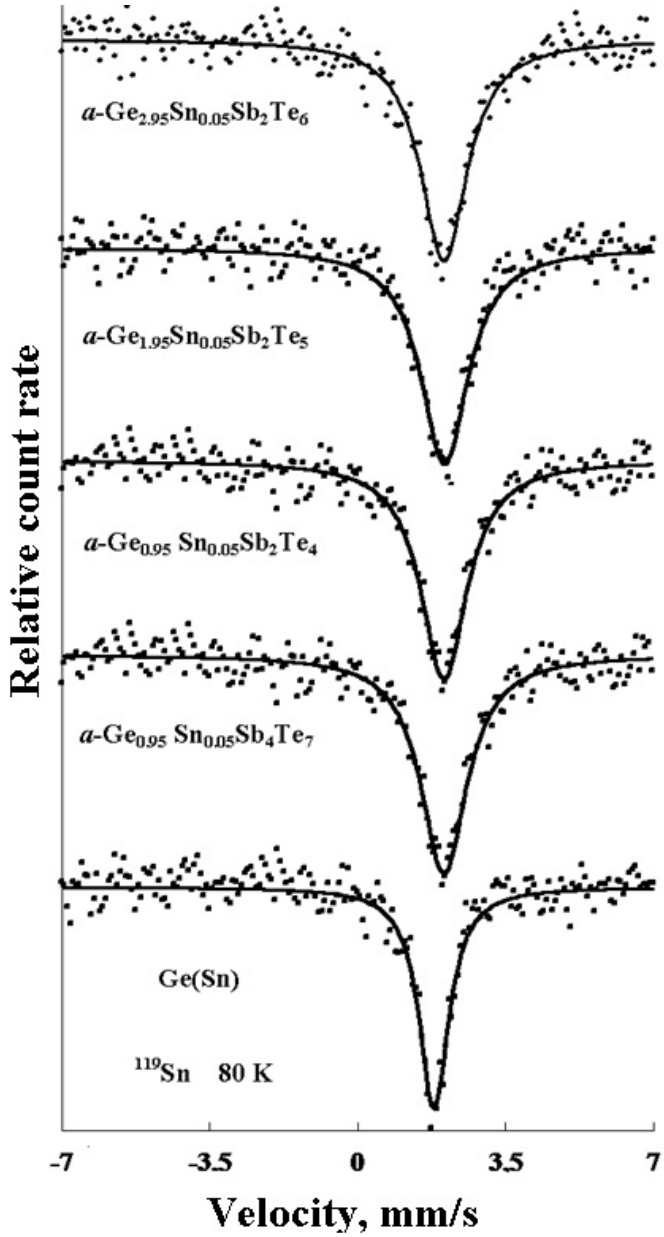

Fig. 2. Mössbauer spectra of ^{119}Sn in Ge(Sn)Sb amorphous films and in the crystalline germanium GeSn

The ^{119}Sn impurity atoms spectra of GeSbTe crystalline films correspond to the ionic compounds of divalent tin. Fig. 1 shows the ^{119}Sn impurity atoms spectrum in the $Ge_{0.98}Sn_{0.02}Te$ compound for which δ = 3.55(3) mm/s and G = 1.36(2) mm/s were obtained. These parameters correspond to divalent six-coordinated tin which isovalently replaces the divalent six-coordinated germanium atoms in the cationic node of the GeTe crystal lattice. GeTe compound crystallizes in a rhombohedrally distorted NaCl-type lattice, hence the broadening of the ^{119}Sn impurity atoms spectrum in the $Ge_{0.98}Sn_{0.02}Te$ solid solution. The broadening of ternary compounds spectra is also related with the presence of a high concentration of stoichiometric vacancies in the cationic sublattice of these compounds.

The data of Mössbauer spectroscopy on ^{119}Sn impurity atoms for Ge(Sn)SbTe crystalline films comply with the results of the X-ray diffraction studies of metastable vacancy-disordered cubic GeSbTe crystalline compounds. Divalent tin Sn^{2+} (electronic configuration is $5s^2p^x$) replaces divalent germanium Ge^{2+} (electronic configuration is $4s^2p^x$) in positions 4 *b* of the rhombohedrally distorted NaCl-type crystal lattice, and there are only tellurium atoms in the nearest environment of six-coordinated germanium atoms. The latter circumstance explains the closeness of the isomer shifts of the ^{119}Sn spectra in the GeSbTe crystalline compounds to the isomer shift of the ^{119}Sn spectrum in the SnTe

 https://www.doi.org/10.33910/2687-153X-2022-4-1-30-35

compound (δ = 3.54(1) mm/s and G = 0. 94(2) mm/s) and also to the isomer shift of the ^{119}Sn impurity atom in the GeTe compound. The broadening of the spectra of *c*-GeSbTe ternary compounds compared to the spectral width of SnTe is due to the rhombohedral distortion of the lattices of *c*-GeSbTe compounds (six Ge-Te bonds at sites with octahedral symmetry are divided into three short and three long bonds, as in a GeTe crystal) as well as to a high concentration of randomly distributed stoichiometric vacancies in the cationic sublattice (Lotnyk et al. 2016; Sun et al. 2007; Urban et al. 2013; Wang et al. 2017; Zhang et al. 2016; Zheng et al. 2019).

The first problem that Mössbauer spectroscopy can solve is the determination of the valence state and local coordination number of germanium atoms in GeSbTe amorphous films. The isomer shifts of the ^{119}Sn spectra of Ge(Sn)Sb amorphous films have values close to the values of the isomer shifts of the spectra of impurity tin atoms ^{119}Sn in monocrystalline germanium (δ = 1.79(1), see Fig. 2) and also close to the measured shift of the spectrum of gray tin α-Sn (δ = 2.10(1)) that form the area of isomer shifts of tetravalent tin compounds with a tetrahedral sp^3 system of chemical bonds. Thus, impurity tin atoms in the structure of Ge(Sn)Sb amorphous films isovalently replace tetravalent germanium atoms, which form a tetrahedral system of chemical bonds (the local coordination number of germanium atoms in amorphous films is four).

The second problem solved using Mössbauer spectroscopy data is the determination of the chemical nature of atoms in the nearest environment of germanium atoms in GeSbTe amorphous films. It should be noted that, if germanium atoms are also present in the nearest environment of germanium atoms (i. e. the formation of Ge-Ge chemical bonds), the isomer shift of the ^{119}Sn spectra of amorphous films should be ~ 1.80 mm/s (as for the spectrum of impurity tin atoms in monocrystalline Ge). At the same time, the spectra of all amorphous films have isomer shifts within δ ~ 2.06–2.09 mm/s. Note that the isomer shifts of the spectra of ^{119}Sn impurity atoms in the $Ge_{1.45}Sn_{0.05}Te_{8.5}$ glassy alloy are of the same range. Here the germanium (tin) atoms are tetravalent, forming a system of sp^3 bonds (their coordination number is four) and having tellurium atoms in the local environment (Seregin et al. 1977; Seregina et al. 1977). This conclusion can be confirmed by the fact that the isomer shift of the ^{119}Sn spectra of Ge(Sn) SbTe amorphous films monotonically increases from 2.03(1) mm/s for the $Ge_3Sb_2Te_6$ compound (contains 27.3 at.% of Ge) to 2.07(1) mm/s for the $GeSb_4Te_7$ compound (contains 8.3 at.% of Ge). Based on all the above, it should be concluded that there are tellurium atoms in the local environment of germanium atoms in the Ge(Sn)SbTe and GeSbTe amorphous films.

Kolobov et al., based on the results of XAFS to describe the order–disorder transition in $Ge_2Sb_2Te_5$ compound films, supposed that a crystalline film amorphization is accompanied by a germanium atom jump from octahedral positions in a crystalline film to tetrahedral positions with four Te atoms in the local environment (Kolobov et al. 2004). However, Baker et al. (Baker et al. 2006; Paesler et al. 2007), also using the EXAFS data, concluded that germanium atoms in $Ge_2Sb_2Te_5$ amorphous films form the Te_3Ge-$GeTe_3$ structural units, where predominant formation of Ge-Ge bonds can be seen. The structure of $Ge_2Sb_2Te_5$ and $GeSb_2Te_4$ amorphous films was also studied using the EXAFS method, in combination with high-energy X-ray diffraction and neutron diffraction, by the authors of (Jóvári et al. 2008). Ge-Ge and Ge-Sb bonds were shown to be present while Te–Te and Sb–Sb bonds were not found. Germanium atoms have a fourfold coordination. Finally, the local structure of the $Ge_2Sb_2Te_5$ amorphous phase was studied using anomalous X-ray scattering near the absorption K-edges of germanium, antimony, and tellurium atoms (Stellhorn et al. 2020). A half of the Ge atoms were found to have an octahedral environment similar to that in a crystalline phase. The remaining half of germanium atoms has tetrahedral symmetry and forms an energy barrier between the amorphous and crystalline phases, providing a long lifetime for the amorphous modification.

The Mössbauer spectroscopy data obtained by us comply with the ideas of the authors of (Kolobov et al. 2004) about the local structure of germanium atoms in $Ge_2Sb_2Te_5$ amorphous films and allow us to extend these results to other GeSbTe amorphous compounds. Tetravalent germanium atoms form a tetrahedral system of chemical bonds in the structural network of the amorphous matrix and have only tellurium atoms in their nearest environment. The conclusion of the authors of (Jóvári et al. 2008) that germanium atoms in $Ge_2Sb_2Te_5$ and $GeSb_2Te_4$ amorphous compounds have fourfold coordination is also confirmed (with the only clarification that this is true for all the GeSbTe amorphous films).

Conclusions

The local environment of atoms in $Ge_3Sb_2Te_6$, $Ge_2Sb_2Te_5$, $GeSb_2Te_4$ and $GeSb_4Te_7$ crystalline and amorphous films was determined by Mössbauer spectroscopy on the ^{119}Sn isotope. The data of Mössbauer spectroscopy on ^{119}Sn impurity atoms for crystalline films comply with the results of the X-ray diffraction studies: divalent tin replaces divalent germanium in a rhombohedrally distorted NaCl-type lattice.

Impurity tin atoms in the structure of GeSnSbTe amorphous films isovalently replace tetravalent germanium atoms, which form a tetrahedral system of chemical bonds (the local coordination number of germanium atoms in GeSbTe amorphous films is four), and the local environment of germanium contains mainly tellurium atoms.

Acknowledgements

I would like to thank my supervisor Prof. Seregin P. P. and Prof. Marchenko A. V. for their consistent support and guidance in carrying out this research.

Conflict of Interest

The author declares that there is no conflict of interest, either existing or potential.

References

Baker, D. A., Paesler, M. A., Lucovsky, G., Taylor, P. C. (2006) EXAFS study of amorphous $Ge_2Sb_2Te_5$. *Journal of Non-Crystalline Solids*, 352 (9-20), 1621–1623. https://doi.org/10.1016/j.jnoncrysol.2005.11.079 (In English)

Bordovskii, G. A., Marchenko, A. V., Nasredinov, F. S. et al. (2021) Messbauerovskie issledovaniya lokal'nogo okruzheniya atomov v amorfnykh i kristallicheskikh plenkakh $Ge_2Sb_2Te_5$ [Mossbauer studies of the local surrounding of atoms in amorphous and crystalline $Ge_2Sb_2Te_5$ films]. *Fizika i khimiya stekla — Glass Physics and Chemistry*, 47 (2), 179–189. https://doi.org/10.31857/S0132665121020037 (In Russian)

Jóvári, P., Kaban, I., Steiner, J., et al. (2008) Local order in amorphous $Ge_2Sb_2Te_5$ and $GeSb_2Te_4$. *Physical Review B*, 77 (3), article 035202. https://doi.org/10.1103/PhysRevB.77.035202 (In English)

Kolobov, A. V., Fons, P., Frenkel, A. I. et al. (2004) Understanding the phase-change mechanism of rewritable optical media. *Nature Materials*, 3, 703–708. https://doi.org/10.1038/nmat1215 (In English)

Ledda, F., Muntoni, C., Rucci, A. et al. (1988) On the metal distribution in the system GeTe-Sb_2Te_3, *Hyperfine Interactions*, 41, 591–594. https://doi.org/10.1007/BF02400460 (In English)

Lencer, D., Salinga, M., Wuttig, M. (2011) Design rules for phase-change materials in data storage applications. *Advanced Materials*, 23 (18), 2030–2058. https://doi.org/10.1002/adma.201004255 (In English)

Lotnyk, A., Ross, U., Bernütz, S. et al. (2016) Local atomic arrangements and lattice distortions in layered Ge-Sb-Te crystal structures. *Scientific Reports*, 6, article 26724. https://doi.org/10.1038/srep26724 (In English)

Marchenko, A. V., Terukov, E. I., Nasredinov, F. S. et al. (2021) Local structure and anti-structural defects of tin in amorphous and crystalline $Ge_2Sb_2Te_5$ films. *Semiconductors*, 55 (1), 1–6. https://doi.org/10.1134/S1063782621010127 (In English)

Paesler, M. A., Baker, D. A., Lucovsky, G. et al. (2007) Bond constraint theory and EXAFS studies of local bonding structures of $Ge_2Sb_2Te_4$, $Ge_2Sb_2Te_5$, and $Ge_2Sb_2Te_7$. *Journal of Optoelectronics and Advanced Materials*, 9 (10), 2996–3001. (In English)

Qiao, C., Guo, Y. R., Wang, J. J. et al. (2019) The local structural differences in amorphous Ge-Sb-Te alloys. *Journal of Alloys and Compounds*, 774, 748–757. https://doi.org/10.1016/j.jallcom.2018.10.011 (In English)

Seregin, P. P., Sivkov, V. P., Nasredinov, F. S. et al. (1977) The influence of the crystal-to-glass transition on the local structure of semiconductors. *Physica Status Solidi (a)*, 39 (2), 437–444. https://doi.org/10.1002/pssa.2210390209 (In English)

Seregina, L. N, Nasredinov, F. S., Melekh, B. T. et al. (1977) Issledovanie lokal'noj struktury stekol v sistemakh kremnij–tellur, germanij–tellur i germanij–tellur–mysh'yak s pomoshch'yu messbauerovskoj spektroskopii na primesnykh atomakh olova [Study of the local structure of glasses in silicon-tellurium, germanium-tellurium and germanium-tellurium-arsenic systems using Mössbauer spectroscopy on impurity tin atoms]. *Fizika i khimiya stekla — Glass Physics and Chemistry*, 3 (4), 328–331. (In Russian)

Stellhorn, J. R., Hosokawa, S., Kohara, S. (2020) Local- and intermediate-range structures on ordinary and exotic phase-change materials by anomalous x-ray scattering. *Analytical Sciences*, 36, 5–9. https://doi.org/10.2116/analsci.19SAR02 (In English)

Sun, Z., Kyrsta, S., Music, D. et al. (2007) Structure of the Ge-Sb-Te phase-change materials studied by theory and experiment. *Solid State Communications*, 143 (4-5), 240–244. https://doi.org/10.1016/j.ssc.2007.05.018 (In English)

Urban, P., Schneider, M., Erra, L. et al. (2013) Temperature dependent resonant X-ray diffraction of single-crystalline $Ge_2Sb_2Te_5$. *CrystEngComm*, 15 (24), 4823–4829. https://doi.org/10.1039/C3CE26956F (In English)

Wang, X.-P., Li, X.-B., Chen, N.-K. et al. (2017) Element-specific amorphization of vacancy-ordered GeSbTe for ternary-state phase change memory. *Acta Materialia*, 136, 242–248. https://doi.org/10.1016/j.actamat.2017.07.006 (In English)

Zhang, B., Wang, X.-P., Shen, Z.-J. et al. (2016) Vacancy structures and melting behavior in rock-salt GeSbTe. *Scientific Reports*, 6, article 25453. https://doi.org/10.1038/srep25453 (In English)

Zheng, Y., Wang, Y., Xin, T. et al. (2019) Direct atomic identification of cation migration induced gradual cubic-to-hexagonal phase transition in $Ge_2Sb_2Te_5$. *Communications Chemistry*, 2, article 13. https://doi.org/10.1038/s42004-019-0114-7 (In English)

Physics of Semiconductors. Physics of thin films

UDC 538.935

EDN ANTHJA
https://www.doi.org/10.33910/2687-153X-2022-4-1-36-41

Resistivity of thin bismuth films under in-plane tensile strain

A. V. Suslov✉[1], V. A. Gerega[1], M. D. Glebov[1], V. M. Grabov[1], V. A. Komarov[1]

[1] Herzen State Pedagogical University of Russia, 48 Moika Emb., Saint Petersburg 191186, Russia

Authors

Anton V. Suslov, ORCID: 0000-0003-1934-245X, e-mail: a.v_suslov@mail.ru

Vasilisa A. Gerega, ORCID: 0000-0003-4235-7713, e-mail: gerega.vasilisa96@gmail.com

Matvey D. Glebov, ORCID: 0000-0002-7817-5746, e-mail: matvejj.glebov@gmail.com

Vladimir M. Grabov, ORCID: 0000-0003-0215-6474, e-mail: vmgrabov@yandex.ru

Vladimir A. Komarov, ORCID: 0000-0002-2482-0885, e-mail: va-komar@yandex.ru

For citation: Suslov, A. V., Gerega, V. A., Glebov, M. D., Grabov, V. M., Komarov, V. A. (2023) Resistivity of thin bismuth films under in-plane tensile strain. *Physics of Complex Systems*, 4 (1), 36–41. https://www.doi.org/10.33910/2687-153X-2022-4-1-36-41 EDN ANTHJA

Received 20 January 2023; reviewed 10 February 2023; accepted 10 February 2023.

Funding: The research was supported by the Ministry of Education of the Russian Federation as part of a state task project No. VRFY-2023-0005.

Abstract. The unique properties of bismuth and bismuth-antimony have attracted extensive attention in scope of strain engineering and straintronics in 2D materials in the past few decades. In this work we tested the technique of measurement of electric properties of bismuth films on glass and silicon substrates deformed by dome bending method. The obtained results show fine agreement with the investigation of films deformed by others techniques and can be used to model in-plane tensile deformation. Considering the use of two substrates of silicon and borosilicate glass, the method makes it possible to obtain continuously changed deformation of film in range up to 0.8 % of relative change of area at room temperature.

Keywords: bismuth, thin films, tensile deformation, resistivity, glass substrate, silicon substrate

Introduction

In recent years, interest in studying the effects caused by the influence of deformation on the physical properties of materials has revived again due to the development of straintronics (Bukharaev et al. 2018). In this regard, semimetals and narrow-gap semiconductors based on bismuth are of particular interest, since transport properties of bismuth films are significantly affected by various factors, in particular, deformations (Aguilera et al. 2015; Suslov et al. 2019b; Wu et al. 2018). This is due to the peculiarities of the bismuth band structure, which is characterized by a small indirect overlap of the valence and conduction bands (~40 mEv), as well as a small direct band gap (~15 mEv) (Jezequel et al. 1997). These features make it possible to smoothly change the parameters of the band structure of the samples during deformation and, consequently, to control their properties. From the experimental point of view, it is of interest to study the effect of in-plane strains on the transport properties of films since, firstly, significant strains can be obtained in the film state, which are not achievable in the bulk crystal (Suslov et al. 2022). Secondly, such deformations are quite easy to create in films since it was shown that the film on the substrate is in a deformed state at temperatures different from the producing temperature due to mismatch between the thermal expansion coefficients (CTE) of the film and the substrate (Suslov et al. 2019a).

In (Hirahara et al. 2012), based on ab-initio calculations, bismuth films on substrates with different lattice constants in the trigonal plane were simulated. The first principle calculations (based on the density functional theory (DFT)) of band structure of a bulk bismuth under various deformations in the trigonal plane were carried out. The strong influence of deformation on the band structure of the material was shown. Under compressive strain in the trigonal plane the energy overlap increased, while under tensile strain it decreased until a semiconductor gap appeared. With DFT, it was shown in (Wu et al. 2018) that, under uniaxial compressive strain of a bulk bismuth along the C_3 axis, a semimetal–semiconductor transition occurs in the region of the lattice constant ratio c/a = 2.41–2.51 with a maximum band gap at c/a = 2.45. In this state, an increase in the Seebeck coefficient and a decrease in thermal conductivity are expected, which, despite a decrease in conductivity, lead to an increase in ZT, which is one of the most important tasks in the development of thermoelectric converters.

As shown in numerous studies, bismuth films on various substrates grow predominantly in such a way that the trigonal axis of the crystal is perpendicular to the substrate plane (Jankowski et al. 2017; Krushelnitckii et al. 2017; Rodil et al. 2017). Thus, the deformations observed in the film samples are compressive or tensile strains in the trigonal plane. Due to the mismatch between the CTE of bismuth and various substrates, both compressive and tensile strains can be obtained. By combining this method and the method of substrate dome bending, it is possible to significantly expand the range of the created deformation (Suslov et al. 2022).

The paper presents the results of a study of the strain dependences of the bismuth films resistivity on borosilicate glass and silicon substrates, which undergo auxiliary in-plane tensile deformation by dome bending of substrate.

Experimental methods

The films were produced in high vacuum (up to 10^{-5} Torr) on borosilicate glass and silicon substrate by thermal evaporation. The surface of silicon substrate was oxidized (the thickness of oxide layer was approximately 1 um). It is shown that the size of bismuth film crystallites can significantly affect the transport properties of charge carriers (Komarov et al. 2019). Thus, oxidizing is crucial because it makes it possible to obtain the similar crystal structure of bismuth films on glass and silicon substrates.

In order to improve crystalline quality of the films, it was produced at 393 K with subsequent annealing at 523 K in 1 hour. During the annealing, the processes of recrystallization and coalescence occur, which lead to enlargement of crystallite size, reducing of crystallographic axes misorientation in adjacent crystallites and mechanical stress relaxation. Therefore, the annealing temperature is considered as the temperature of film formation.

The surface morphology was investigated by means of NT-MDT Solver Pro P47 atomic force microscope (AFM) of Herzen University shared core facilities in semicontact mode. In order to highlight the crystalline boundaries, the chemical etching with nitric and acetic acids solution was used (Demidov et al. 2017).

The crystal structure was investigated by X-ray diffraction (XRD) analysis technics by means of X-ray diffractometer DRON–7 of Herzen University shared core facilities using the classical Bregg-Brentano (θ–2θ) geometry. The shift of diffraction lines, corresponding to the trigonal plane of the single-crystal, indicates the change in the c-lattice constant (in the hexagonal elementary cell).

As mentioned previously, the discrepancy of the CTE of the film and the substrate leads to in-plane deformation at the temperature different from the formation temperature. The relative in-plane film area deformation can be expressed as

$$\frac{\Delta S}{S} = e^{2\int_{T_f}^{T} \alpha_s dT - \alpha_f dT} - 1$$

where α_s, α_f—substrate and film materials' CTEs, T_f—film formation temperature.

Table 1 shows the relative deformation of thin bismuth films on borosilicate glass and silicon substrate at 300 K and 77 K according to the above-mentioned formula as well as CTE of the used materials. The CTE of bismuth is anisotropic, so Table 1 shows its value in the trigonal plane. The CTE of borosilicate glasses has a wide range of values, so it was measured directly on the substrates used.

Table 1. Thermal expansion coefficients of materials

	α, 10^{-6} K^{-1}	ΔS/S at 300 K, %	ΔS/S at 77 K, %
Silicon	2.64*	0.47	0.95
Borosilicate glass	7.8	0.18	0.38
Bismuth	11.2**	—	—

Note: *—(Batchelder, Simmons 1964; Roberts, White 1986); **—(Cave, Holroyd 1960; Bunton, Weintroub 1969).

The range of tensile deformation can be expanded by auxiliary mechanical deformation of substrate, e. g., dome bending of the substrate. The method of dome bending is described in (Suslov et al. 2022) and based on stretching of the outer surface of the bended substrate on which the film is deposited. In the first approximation, the film deformation can be considered as an in-plane tensile strain, since the bending curvature radii are quite large and the film area is relatively small. The scheme of substrate bending is shown in Fig. 1.

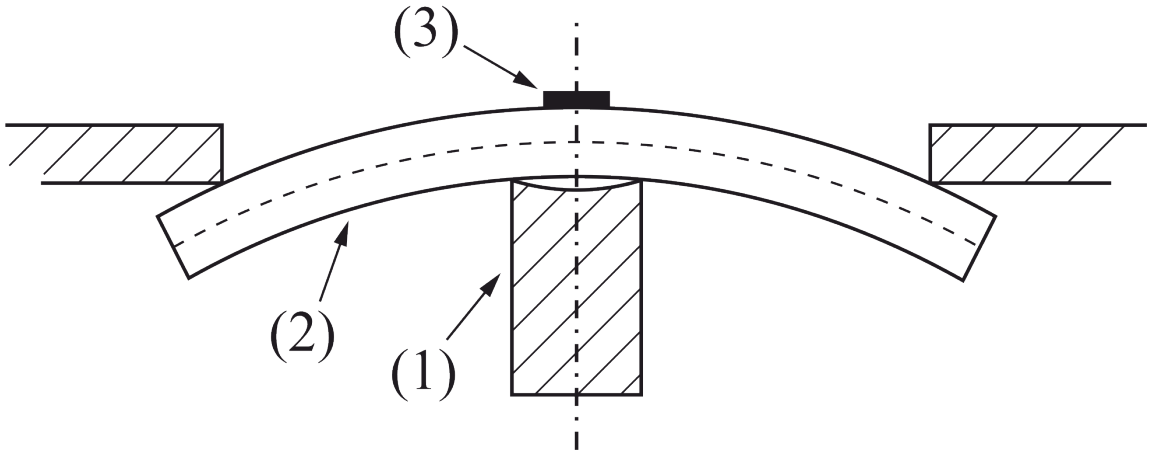

Fig. 1. The scheme of dome bending of the substrate. (1) shaft; (2) substrate; (3) deposited thin film

In the work we significantly improved the mechanical rigidity of the device for dome bending of the substrate. That made it possible to clearly determine the starting moment of dome bending.

In the framework of this work we investigate the resistivity of thin films relative to temperature and magnitude of deformation. The measurements were performed on samples powered by constant current at constant temperature. Temperature dependencies were obtained in the range of 77–300 K. Magnitude of in-plane deformation by dome bending corresponds to 0.8 % by area.

Results and discussion

By means of XRD analysis the preferential orientation of the trigonal axis of texture was determined to be perpendicular to the surface plane. Lattice constants *c* indicate that the silicon substrate stretches the film stronger than the glass substrate.

Fig. 2 shows the surface morphology of films on glass and silicon substrates. Despite the similarity of the average crystallite size, there is enhanced misorientation of the trigonal axis in films on the silicon substrate. It is shown clearly by the shape of grow figures—the deviation from the equilateral triangle shows the inclination of the trigonal axis. But the deviation does not exceed 15°, which was found out by means of XRD. The average size of film crystallites on both substrates is 2–3 μm in the entire range of investigated thicknesses, i.e., it exceeds the film thickness. The same size of crystallites ensures

 https://www.doi.org/10.33910/2687-153X-2022-4-1-36-41

the same ratio of the contributions of the scattering of charge carriers on the film surface and grain boundaries in films on different substrates (Komarov et al. 2019).

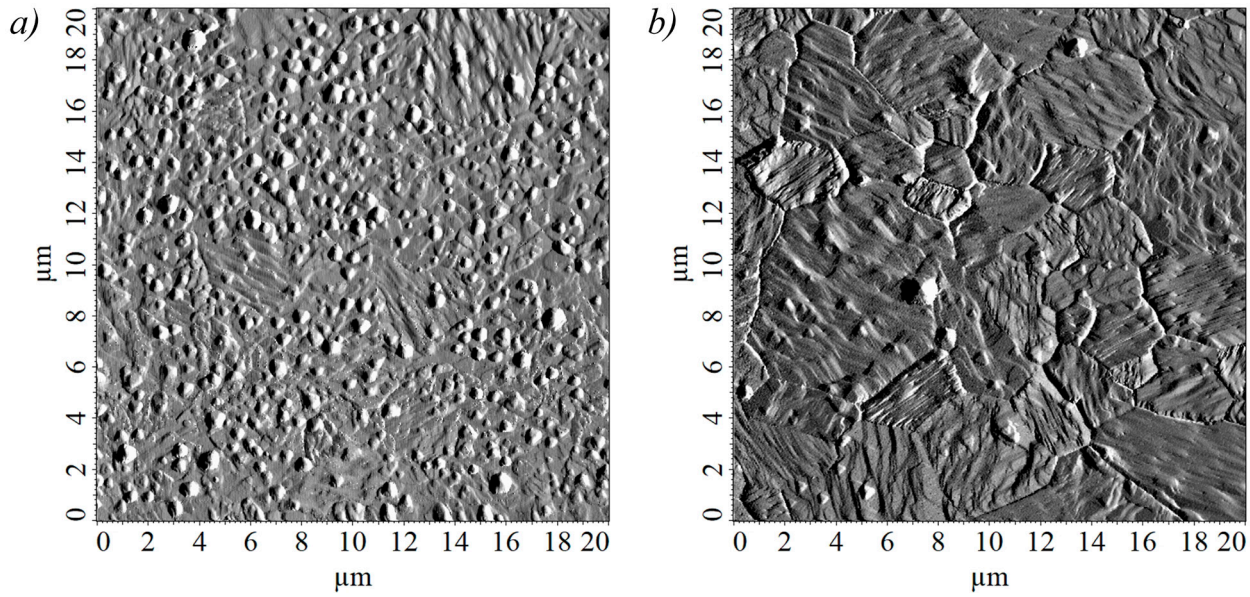

Fig. 2. AFM scan of 1000 nm thick bismuth film on (a) glass substrate; (b) silicon substrate

Fig. 3 shows the temperature dependencies of resistivity, relative to the value at 300 K, of bismuth films on glass and silicon substrates. Such representation allows to eliminate from analysis the difference of resistivity due to the difference in the crystal structure. The films on the silicon substrate have enhanced resistivity relative to resistivity on the glass substrate. The difference increases as the temperature decreases. It strongly correlates with the increase of deformation magnitude due to the difference in CTE of substrates.

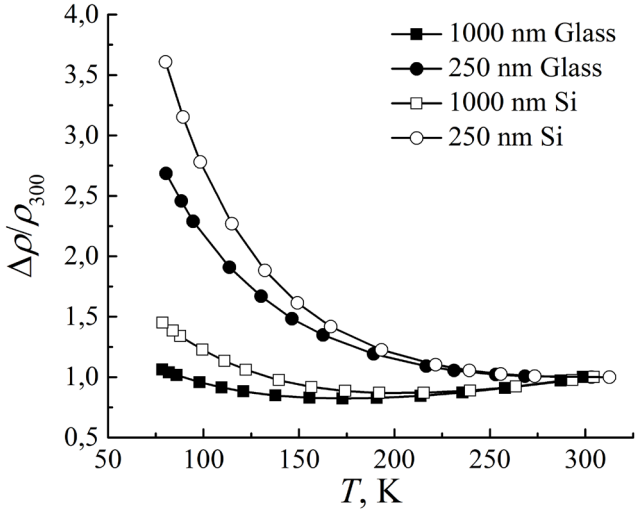

Fig. 3. Temperature dependencies of resistivity of bismuth films of 1000 nm and 250 nm thickness on the glass and the silicon substrate

The dependence of resistivity on deformation produced by dome bending is shown in Fig. 4 by example of 1000 nm bismuth films. The magnitude of deformation expressed as relative change of film

area and was calculated by formula (1) and indirectly confirmed by XRD, according to *c*/*a* ratio (Suslov et al. 2022). The resistivity increases with increasing magnitude of deformation. Considering the thickness of the films, the resistance increases by approximately 0.12 Ohm by percent of relative area stretch. Because of difference in the crystal structure, there is a shift of resistivity in the film on silicon. However, the slope of curves shows possibility of their "stitching". So, by using two substrates of silicon and glass, one can obtain the continuous film deformation in the range of magnitude up to 0.8 % (by area) at room temperature. At the temperature of 77 K the deformation produced by difference of the film and substrate CTEs increases, consequently, the range of deformation magnitude is supposed to be exceeded.

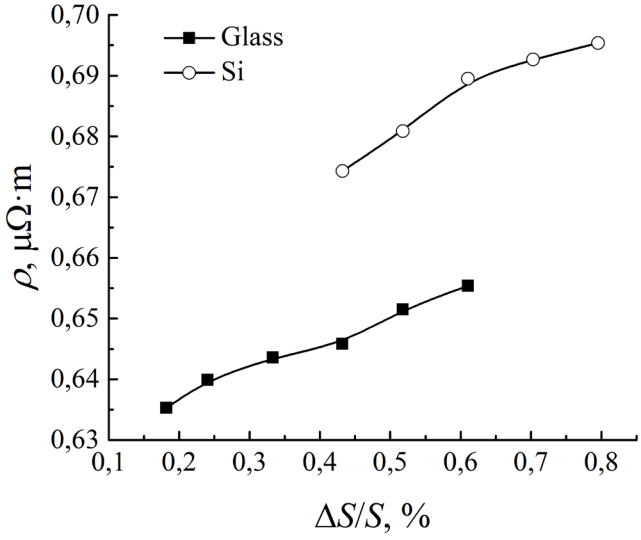

Fig. 4. The dependence of resistivity of bismuth film of 1000 nm thickness on glass and silicon substrates in condition of dome bending

The authors propose one more way to ensure the relevancy of using the dome bending method to model the in-plane tensile deformation by investigation of the crystal structure of films on bended substrates at temperature 77 K by means of XRD, but it is beyond the scope of this work.

Conclusions

In this work we tested the technique of measurement of electric properties of films on glass and silicon substrates deformed by dome bending method. The obtained results show fine agreement with resistivity data of thin films on different substrates and indicate the relevancy of using the dome bending method to expand the range of thin films tensile deformation relative to deformation occurred due to difference in CTE of film and substrate materials.

Conflict of Interest

The authors declare that there is no conflict of interest, either existing or potential.

Author Contributions

Anton Suslov—development of a setup for measurements of the films transport properties under conditions of the substrate dome bending, XRD, data analysis, editing; Vasilisa Gerega—data analysis, preparation of the manuscript and figures; Matvey Glebov—samples producing, AFM and electrical properties measurements; Vladimir Grabov—editing, supervision; Vladimir Komarov—research concept development, data analysis, editing, supervision. All authors have read and agreed to the published version of the manuscript.

 https://www.doi.org/10.33910/2687-153X-2022-4-1-36-41

References

Aguilera, I., Friedrich, C., Blügel, S. (2015) Electronic phase transitions of bismuth under strain from relativistic self-consistent GW calculations. *Physical Review B*, 91 (12), article 125129. https://doi.org/10.1103/PhysRevB.91.125129 (In English)

Batchelder, D. N., Simmons, R. O. (1964) Lattice constants and thermal expansivities of silicon and of calcium fluoride between 6 and 322 K. *The Journal of Chemical Physics*, 41 (8), 2324–2329. https://doi.org/10.1063/1.1726266 (In English)

Bukharaev, A. A., Zvezdin, A. K., Pyatakov, A. P., Fetisov, Y. K. (2018) Straintronics: A new trend in micro- and nanoelectronics and materials science. *Physics-Uspekhi*, 61 (12), 1175–1212. https://doi.org/10.3367/ufne.2018.01.038279 (In English)

Bunton, G. V., Weintroub, S. (1969) The thermal expansion of antimony and bismuth at low temperatures. *Journal of Physics C: Solid State Physics*, 2 (1), article 116. https://doi.org/10.1088/0022-3719/2/1/317 (In English).

Cave, E. F., Holroyd, L.V. (1960) Thermal expansion coefficients of bismuth. *Journal of Applied Physics*, 31 (8), article 1357. https://doi.org/10.1063/1.1735842 (In English)

Demidov, E. V., Komarov, V. A., Krushelnitckii, A. N., Suslov, A. V. (2017) Measurement of the thickness of block-structured bismuth films by atomic-force microscopy combined with selective chemical etching. *Semiconductors*, 51 (7), 840–842. https://doi.org/10.1134/S1063782617070065 (In English)

Hirahara, T., Fukui, N., Shirasawa, T. et al. (2012) Atomic and electronic structure of ultrathin Bi(111) films grown on Bi_2Te_3(111) substrates: Evidence for a strain-induced topological phase transition. *Physical Review Letters*, 109 (22), article 227401. https://doi.org/10.1103/PhysRevLett.109.227401 (In English)

Jankowski, M., Kaminski, D., Vergeer, K. et al. (2017) Controlling the growth of Bi(110) and Bi(111) films on an insulating substrate. *Nanotechnology*, 28 (15), article 155602. https://doi.org/10.1088/1361-6528/aa61dd (In English)

Jezequel, G., Thomas, J., Pollini, I. (1997) Experimental band structure of semimetal bismuth. *Physical Review B*, 56 (11), 6620–6626. https://doi.org/10.1103/PhysRevB.56.6620 (In English)

Komarov, V. A., Grabov, V. M., Suslov, A. V. et al. (2019) The Hall and seebeck effects in bismuth thin films on mica substrates in the temperature range of 77–300 K. *Semiconductors*, 53 (5), 593–598. https://doi.org/10.1134/S1063782619050105 (In English)

Krushelnitckii, A. N., Demidov, E. V., Ivanova, E. K. et al. (2017) Dependence of the surface morphology of ultrathin bismuth films on mica substrates on the film thickness. *Semiconductors*, 51 (7), 876–878. https://doi.org/10.1134/S1063782617070211 (In English)

Roberts, R. B., White, G. K. (1986) Thermal expansion of fluorites at high temperatures. *Journal of Physics C: Solid State Physics*, 19 (36), 7167–7172. https://doi.org/10.1088/0022-3719/19/36/008 (In English)

Rodil, S. E., Garcia-Zarco, O., Camps, E. et al. (2017) Preferential orientation in bismuth thin films as a function of growth conditions. *Thin Solid Films*, 636, 384–391. https://doi.org/10.1016/j.tsf.2017.06.048 (In English)

Suslov, A. V., Gerega, V. A., Grabov, V. M. et al. (2022) Deformation of thin films of semimetals by the dome bending method of the substrate. *Semiconductors*, 56 (1), 22–24. https://doi.org/10.1134/S1063782622020142 (In English)

Suslov, A. V., Grabov, V. M., Komarov, V. A. et al. (2019a) Methods of experimental studying the galvanomagnetic properties of thin semimetals films under conditions of plane stretch. *Journal of Physics Conference Series*, 1281 (1), article 012084. https://doi.org/10.1088/1742-6596/1281/1/012084 (In English)

Suslov, M. V., Grabov, V. M., Komarov, V. A. et al. (2019b) The thermoelectric power of $Bi_{1-x}Sb_x$ films ($0 \le x \le 0.15$) on mica and polyimide substrates in the temperature range of 77–300 K. *Semiconductors*, 53 (5), 589–592. https://doi.org/10.1134/S1063782619050257 (In English)

Wu, C. Y., Han, J. C., Sun, L. et al. (2018) Effects of trigonal deformation on electronic structure and thermoelectric properties of bismuth. *Journal of Physics. Condensed Matter*, 30 (28), article 285504. https://doi.org/10.1088/1361-648X/aacab9 (In English)

Summaries in Russian / Информация о статьях на русском языке

Физика конденсированного состояния

РОЛЬ ПОЛЯРНЫХ РЕЛАКСАТОРОВ В ФОРМИРОВАНИИ ПЬЕЗОЭЛЕКТРИЧЕСКОГО СОСТОЯНИЯ В СОПОЛИМЕРЕ ВИНИЛИДЕНФТОРИД-ТЕТРАФТОРЭТИЛЕН

Гороховатский Юрий Андреевич, Темнов Дмитрий Эдуардович, Сотова Юлия Ильинична

Аннотация. В работе проведено исследование короноэлектретного и пьезоэлектрического состояния полимерных пленок сополимера винилиденфторид-тетрафторэтилен (П(ВДФ-ТФЭ)) на предмет связи между данными состояниями. Ранее было определено, что в исследуемых объектах имеется два сорта полярных структур, отличных по значениям энергии активации и частотного фактора. Приведено подробное описание применения численного метода обработки экспериментальных кривых термостимулированных токов короткого замыкания — метода слабой регуляризации Тихонова — позволяющего определить параметры полярных структур обоих сортов. Показано, что ключевую роль в процессе формирования пьезоэлектрического состояния в П(ВДФ-ТФЭ) играют полярные структуры с меньшей энергией активации.

Ключевые слова: электретное состояние, поливинилиденфторид, термоактивационная спектроскопия, метод слабой регуляризации Тихонова, пьезоэлектрический эффект

Для цитирования: Gorokhovatsky, Yu. A., Temnov, D. E., Sotova, Yu. I. (2023) The role of polar relaxers in the formation of the piezoelectric state in the vinylidene fluoride-tetrafluoroethylene copolymer. *Physics of Complex Systems*, 4 (1), 3–9. https://www.doi.org/10.33910/2687-153X-2022-4-1-3-9 EDN YRXKOW

ЭЛЕКТРОФИЗИЧЕСКИЕ СВОЙСТВА ПОЛИМЕРНЫХ МЕМБРАН С ВКЛЮЧЕНИЕМ В ИХ МАТРИЦУ МЕМБРАН СОЕДИНЕНИЙ РЕДКОЗЕМЕЛЬНЫХ МЕТАЛЛОВ

Лапатин Николай Анатольевич, Кастро Арата Рене Алехандро, Карулина Елена Анатольевна, Тихон Вадимович Резцов

Аннотация. Методом диэлектрической спектроскопии в широком интервале частот (f = 100 Гц…10^5 Гц) и температур (T = 273 K…403 K). была исследована перфтосульфоновая мембран в исходном и модифицированном солью хлорида тербия (III). Модификация мембраны осуществлялась путем ионно-обменной сорбции из водного раствора соли в течение нескольких часов до достижения равновесного значения. Контроль сорбции проводили спектрофотометрически. В ходе диэлектрического измерения были получены данные о проводимости исследуемых образцов и обнаружен ее прыжковый механизм.

Измерение фактора диэлектрических потерь ε” в слоях позволило выявить существование релаксационного процесса, приводящего к релаксационным потерям в образцах

Ключевые слова: перфторсульфоновая мембрана, модифицирование, редкоземельные металлы, диэлектрическая спектроскопия, проводимость

Для цитирования: Lapatin, N. A., Castro Arata, R. A., Karulina, E. A., Reztsov, T. V. (2023) Electrophysical properties of polymer membranes with the introduction of rare-earth metal compounds into membrane matrix. *Physics of Complex Systems*, 4 (1), 10–16. https://www.doi.org/10.33910/2687-153X-2022-4-1-10-16 EDN QBUBEL

Теоретическая физика

СТОЛКНОВЕНИЯ ЧАСТИЦ В ПРОЦЕССЕ ГРАВИТАЦИОННОГО КОЛЛАПСА МЕТРИКИ ВАЙДЬЯ

Вертоградов Виталий Дмитриевич

Аннотация.

Энергия центра масс двух сталкивающихся частиц, в метрике Шварцшильда, может быть неограниченно большой если мы рассматриваем лобовое столкновение частиц. Для такого процесса, одна частица должна двигаться вдоль белодырных геодезических, а другая должна двигаться навстречу вдоль чернодырной геодезической. Такое возможно, если рассматривается

модель гравитационного коллапса. В этой статье, мы рассматриваем хорошо известную модель гравитационного коллапса метрики Вайдья, результатом которого является формирование голой сингулярности и исследуем вопрос о столкновении частиц вблизи границы коллапсирующего вещества. Мы рассматриваем энергию центра масс сталкивающихся частиц. Одна частица летит по геодезической, начинающейся в голой сингулярности, а другая падает на коллапсирующее вещество. Мы показываем, что энергия центра масс неограничена, если столкновение происходит в близи конформного горизонта Киллинга.

Ключевые слова: гравитационный коллапс, столкновение частиц, метрика Вайдья, голая сингулярность, конформная симметрия

Для цитирования: Vertogradov, V. D. (2023) On particle collisions during gravitational collapse of Vaidya spacetimes. *Physics of Complex Systems*, 4 (1), 17–23. https://www.doi.org/10.33910/2687-153X-2022-4-1-17-23 EDN JTHSXS

К ВОПРОСУ О ПРОЦЕССЕ ВЗАИМНОЙ НЕЙТРАЛИЗАЦИИ В СТОЛКНОВЕНИЯХ МАГНИЯ С ИЗОТОПАМИ ВОДОРОДА

Воронов Ярослав Владимирович, Беляев Андрей Константинович

Аннотация. В данной работе методом токов вероятности рассчитаны сечения процессов взаимной нейтрализации при столкновениях магния с дейтерием в диапазоне энергий столкновения 0,001–100 эВ. Особое внимание уделено энергиям столкновения в окрестности значения Ecol = 0,059 эВ. Также рассчитаны парциальные константы скорости процессов взаимной нейтрализации для температуры T = 6000 K, и проведено сравнение результатов, полученных методом токов вероятности, с данными, полученными ранее. Показано, что рассчитанные методом токов вероятности результаты разумно согласуются с предыдущими теоретическими и экспериментальными данными.

Ключевые слова: атомные данные, атомные процессы, перенос заряда, магний, взаимная нейтрализация

Для цитирования: Voronov, Ya. V., Belyaev, A. K. (2023) On mutual neutralization process in collisions of magnesium with hydrogen isotopes. *Physics of Complex Systems*, 4 (1), 24–29. https://www.doi.org/10.33910/2687-153X-2022-4-1-24-29 EDN KCPGCI

Физика полупроводников

ЛОКАЛЬНОЕ ОКРУЖЕНИЕ АТОМОВ ГЕРМАНИЯ В АМОРФНЫХ И КРИСТАЛЛИЧЕСКИХ ПЛЁНКАХ $GE_3SB_2TE_6$, $GE_2SB_2TE_5$, $GESB_2TE_4$ И $GESB_4TE_7$

Петрушин Юрий Александрович

Аннотация. Методом мёссбауэровской спектроскопии на изотопе ^{119}Sn определено валентное состояние и локальное окружение атомов германия в аморфных и кристаллических плёнках $Ge_3Sb_2Te_6$, $Ge_2Sb_2Te_5$, $GeSb_2Te_4$ и $GeSb_4Te_7$. В кристаллических плёнках двухвалентный германий находится в октаэдрических позициях ромбоэдрически искажённой решётке типа NaCl, тогда как в аморфных плёнках четырёхвалентные атомы германия образуют тетраэдрическую систему химических связей. Во всех плёнках в ближайшем окружении германия находятся преимущественно атомы теллура.

Ключевые слова: локальная структура, мёссбауэровская спектроскопия, аморфные и кристаллические пленки, валентное состояние, локальное окружение

Для цитирования: Petrushin, Yu. A. (2023) Local environment of germanium atoms in $Ge_3Sb_2Te_6$, $Ge_2Sb_2Te_5$, $GeSb_2Te_4$ and $GeSb_4Te_7$ amorphous and crystalline films. *Physics of Complex Systems*, 4 (1), 30–35. https://www.doi.org/10.33910/2687-153X-2022-4-1-30-35 EDN KJGEWB

ВЛИЯНИЕ ПЛОСКОСТНОГО РАСТЯЖЕНИЯ НА УДЕЛЬНОЕ СОПРОТИВЛЕНИЕ ТОНКИХ ПЛЕНОК ВИСМУТА

Суслов Антон Владимирович, Герега Василиса Александровна, Глебов Матвей Дмитриевич, Грабов Владимир Минович, Комаров Владимир Алексеевич

Аннотация. Уникальные свойства висмута и системы висмут-сурьма привлекают все более внимание исследователей в области стрейнтроники и деформационной инженерии в двухмерных материалах в последние десятилетия. В рамках данной работы была проведена апробация

исследования удельного сопротивления пленок висмута на подложках из боросиликатного стекла и кремния деформированных методом купольного изгиба. Полученные результаты хорошо согласуются с результатами исследования пленок, деформированных другими методами, и может быть применен для моделирования плоскостной деформации пленки. Учитывая использование двух подложек, метод позволяет получить возможность получения непрерывных зависимостей свойств пленок от деформации в диапазоне до 0,8 % (относительного изменения площади) при комнатной температуре.

Ключевые слова: висмут, тонкие пленки, деформация растяжения, удельное сопротивление, стеклянная подложка, кремниевая подложка

Для цитирования: Suslov, A. V., Gerega, V. A., Glebov, M. D., Grabov, V. M., Komarov, V. A. (2023) Resistivity of thin bismuth films under in-plane tensile strain. *Physics of Complex Systems*, 4 (1), 36–41. https://www.doi.org/10.33910/2687-153X-2022-4-1-36-41 EDN ANTHJA